



HAL
open science

Petrographic and C & O isotopic characteristics of the earliest stages of aqueous alteration of CM chondrites

Lionel Vacher, Yves Marrocchi, Johan Villeneuve, Maximilien Verdier-Paoletti, Matthieu Gounelle

► To cite this version:

Lionel Vacher, Yves Marrocchi, Johan Villeneuve, Maximilien Verdier-Paoletti, Matthieu Gounelle. Petrographic and C & O isotopic characteristics of the earliest stages of aqueous alteration of CM chondrites. *Geochimica et Cosmochimica Acta*, 2017, 213, pp.271-290. 10.1016/j.gca.2017.06.049 . hal-04028478

HAL Id: hal-04028478

<https://hal.science/hal-04028478>

Submitted on 14 Mar 2023

HAL is a multi-disciplinary open access archive for the deposit and dissemination of scientific research documents, whether they are published or not. The documents may come from teaching and research institutions in France or abroad, or from public or private research centers.

L'archive ouverte pluridisciplinaire **HAL**, est destinée au dépôt et à la diffusion de documents scientifiques de niveau recherche, publiés ou non, émanant des établissements d'enseignement et de recherche français ou étrangers, des laboratoires publics ou privés.



Distributed under a Creative Commons Attribution - NonCommercial - NoDerivatives 4.0 International License

31 aqueous alteration, before Type 0 Ca-carbonates. Isotopic measurements show that Paris' Ca-
32 carbonates have $\delta^{13}\text{C}$ values that range from 19 to 80 ‰ (PDB), $\delta^{18}\text{O}$ values that range from
33 29 to 41 ‰, and $\delta^{17}\text{O}$ values that range from 13 to 24 ‰ (SMOW). According to the $\delta^{13}\text{C}$ -
34 $\delta^{18}\text{O}$ values of Paris' Ca-carbonates, we developed a new alteration model that involves (i) the
35 equilibration of a primordial $^{17,18}\text{O}$ -rich water (PW) with ^{16}O -rich anhydrous silicates and (ii)
36 varying contribution of ^{12}C - and ^{13}C -rich soluble organic matter (SOMs). It also suggests that
37 many parameters control the C and O isotopic composition of Ca-carbonates, the principals
38 being the degree of isotopic equilibration between the PW and the anhydrous silicates, the
39 respective contribution of ^{12}C and ^{13}C -rich SOMs as well as the thermal evolution of CM
40 parent bodies. Consequently, we suggest that CM Ca-carbonates could record both positive
41 and negative $\delta^{13}\text{C}$ - $\delta^{18}\text{O}$ relationships, but a systematic correspondence is probably absent in
42 CM chondrites due to the large number of factors involved in generating the isotopic
43 characteristics of Ca-carbonates. From recent reports of the C-isotopic compositions of SOM
44 in CM chondrites, we propose that water-soluble organic compounds were the most probable
45 source of ^{13}C enrichment in the majority of CM carbonates.

46

47 **1. Introduction**

48 The solar system formed 4.567 billion years ago (Connelly et al., 2012) *via* the
49 collapse of a dense molecular cloud leading to the creation of a protoplanetary disk (Safronov,
50 1969; Boss and Goswami, 2006). The physicochemical evolution of the disk led to the
51 formation of several mineral assemblages: calcium- and aluminum-rich refractory inclusions
52 (CAIs), chondrules, Fe-Ni metal and sulfide beads, and a suite of very fine-grained crystalline
53 and amorphous materials. These components accreted to form the asteroidal parent bodies
54 that are the sources of unequilibrated meteorites (i.e., chondrites). Depending on the radial
55 distance to the early Sun and the turbulence within the disk (Johansen et al., 2015), sub-

56 millimeter-sized water ice grains of solar system (Alexander et al., 2012) and interstellar
57 origin (Piani et al., 2015; Vacher et al., 2016) may have comprised a significant proportion of
58 asteroids and comets (Brearley, 2006; Alexander et al., 2015). Heat released from the decay
59 of ^{26}Al led to melting of the water ice, resulting in the establishment of significant fluid
60 alteration processes within asteroids and shortly after their accretion (Grimm and McSween,
61 1989; Wilson et al., 1999; Petit et al., 2009; Dyl et al., 2012; Doyle et al., 2015)

62 The physicochemical conditions under which hydrated chondrites were aqueously
63 altered are poorly constrained (Brearley, 2006), in particular the length scale of liquid water
64 flow. Numerical simulations of asteroidal aqueous alteration in an open system have predicted
65 large-scale flow over tens of km (Grimm and McSween, 1989; Young et al., 1999, 2003;
66 Cohen and Coker, 2000; Coker and Cohen, 2001; Young, 2001a,b, 2004; McSween et al.,
67 2002; Travis and Schubert, 2005; Grimm, 2007). Nevertheless, these results are difficult to
68 reconcile with petrographic and geochemical observations of meteorites. There is little
69 evidence for the redistribution of soluble elements within chondrites at scale greater than 100
70 μm , thus suggesting that aqueous alteration processes are mostly isochemical (Kerrige et al.,
71 1979; McSween, 1979; Grossman et al., 2000, 2002; Grossman and Alexander, 2004).
72 Moreover, CI chondrites, whose average compositions are similar to that of the solar
73 photosphere (Palme et al., 2014), show the higher degree of alteration. The apparent paradox
74 between the numerical models of fluid and thermal alteration of asteroids and petro-
75 geochemical observations might be due to a significant overestimation of the permeability of
76 chondrites (Bland et al., 2009). Bland et al. (2009) argued that numerical simulations strongly
77 depend on the permeability of chondrites, which is four to eight orders of magnitude lower
78 than previously estimated (Grimm and McSween, 1989; Bland et al., 2009). Taking this re-
79 evaluation into account, the revised numerical simulations suggest that liquid water was
80 transported in the range of 10s to 100s of μm (Bland et al., 2009), a finding which is

81 consistent with the small-scale of alteration observed within the least altered chondrites
82 (Pignatelli et al., 2016). Nevertheless, the early stages of alteration remain poorly understood
83 (Le Guillou et al., 2015) especially in terms of (i) the order of appearance of secondary
84 minerals and the relationships between them, and (ii) the isotopic compositions of the altering
85 fluids.

86 CM carbonaceous chondrites have clear evidence for the action of fluids and impact
87 brecciation in the early Solar System (Metzler et al., 1992; Zolensky et al., 1997; Brearley,
88 2006). These chondrites are characterized by a large scale of aqueous alteration degrees
89 (Rubin et al., 2007), from less altered (CM 2.7; Hewins et al., 2014; Marrocchi et al., 2014;
90 Rubin et al., 2015) to heavily altered (i.e., CM 2.0). CMs commonly contain a wide range of
91 secondary mineral phases that were likely produced through parent-body processes, for
92 example phyllosilicates, magnetites, carbonates and Fe-Ni sulfides (Zolensky et al., 1997;
93 Brearley, 2006). However, the secondary phases that are the most abundant of the CM
94 chondrites are tochilinite ($6\text{Fe}_{0.9}\text{S}\cdot 5(\text{Mg}, \text{Fe}^{2+}(\text{OH})_2)$ - cronstedtite
95 ($(\text{Fe}^{2+}_2\text{Fe}^{3+})_3(\text{Fe}^{3+}\text{Si})\text{O}_5(\text{OH})_4$) associations (hereafter referred as TCI for Tochilinite-
96 Cronstedtite Intergrowths) (Pignatelli et al., 2016, 2017), which occur as complex, irregular-
97 shaped intergrowths dispersed throughout the matrix (Tomeoka and Buseck, 1985; Rubin et
98 al., 2007). TCIs are commonly observed in close association with grains of calcium
99 carbonates (calcite and aragonite), mostly as irregular rims surrounding or penetrating the
100 carbonates (Browning and Bourcier, 1998; Benedix et al., 2003; Lee and Ellen, 2008; De
101 Leuw et al., 2010; Lindgren et al., 2011; Lee et al., 2013, 2014; Fujiya et al., 2015). The
102 textural relationship between TCIs and Ca-carbonates suggests that TCIs are Ca-carbonates
103 pseudomorphs (Lee et al., 2014), but the opposite reaction is also thermodynamically possible
104 (Browning and Bourcier, 1998). Thus, the chronology of the formation of secondary
105 mineralogical assemblages remains largely un-constrained.

106 Over the last years, several studies have focused on the Paris chondrite, the least
107 altered CM chondrite known to date (Bourot-Denise et al., 2010; Hewins et al., 2014;
108 Marrocchi et al., 2014; Rubin, 2015; Leroux et al., 2015; Pignatelli et al., 2016; Vacher et al.,
109 2016). Although Paris has been classified as a CM 2.7 (Marrocchi et al., 2014), relatively
110 unaltered regions display characteristics corresponding to a subtype 2.9 with abundant
111 proportions of Fe-Ni metal beads and pristine matrix (Hewins et al., 2014; Leroux et al.,
112 2015; Rubin, 2015). Thus, Paris offer an unique opportunity to better characterize the early
113 stages of fluid alteration in CM chondrites (Pignatelli et al., 2016, 2017). Paris contains a
114 significant porportion of Ca-carbonates ($\approx 2\%$; Marrocchi et al., 2014) whose O-isotopic
115 compositions fall along the continuous trend defined by CM chondrites (Vacher et al., 2016;
116 Verdier-Paoletti et al., 2017). However, some Ca-carbonates have peculiar O-isotopic
117 compositions that suggest the accretion of few percent of water ice grains coming from the
118 outer part of the Solar System (Vacher et al., 2016). This is supported by the distinct C/H vs.
119 D/H correlation reported for the Paris' matrix compared to the other CM chondrites (Piani et
120 al., 2017). Taken together, these results support a dual origin of water ice grains in the CM-
121 accretion region with contributions either from the inner and outer regions of the Solar
122 System. The detection of interstellar water ices in Paris could be linked to its low H₂O
123 concentration relative to other CMs (i.e., 4.8 wt.% vs. ≈ 9 wt.%; Rubin et al., 2007; Vacher et
124 al., 2016) which would preclude the dilution of ^{17,18}O- and D-rich water ices by local water
125 during the alteration processes. Consequently, Paris could also have kept the record of C-
126 bearing inorganic ices from the outer part of the Solar System (Ciesla and Sandfort, 2012).
127 However, the C isotopic composition of the Paris' carbonates has not been determined yet
128 while it would bring important information on the alteration conditions and the source of
129 carbon involves in the precipitation of carbonates (Fujiya et al., 2015). Previous studies
130 revealed than CI, CR and CM carbonates have ¹³C-enriched heterogeneous isotopic

131 compositions ranging from 5 to 80 ‰ (Grady et al., 1988; Alexander et al., 2015; Fujiya et
132 al., 2015; Tyra et al., 2016). The process(es) at the origin of the ¹³C-enrichment and isotopic
133 variability have remained unclear but could be related to the presence of inorganic ices from
134 the outer part of the Solar System (Ciesla and Sandfort, 2012) and/or open system fluid
135 alteration that would generate escape of ¹³C-depleted methane (Guo and Eiler, 2007). In order
136 to better understand the possible source(s) of oxygen and carbon for carbonates, we report a
137 combined petrographic and C & O isotopic study of the Paris chondrite. In addition, a specific
138 attention has been paid to the textural relationships between TCIs and Ca-carbonates and to
139 the *in situ* determination of C and O-isotopic compositions of Ca-carbonates in the context of
140 their surrounding mineralogy.

141

142 **2. Material and methods**

143 ***2-1 Petrographic and mineralogical characterizations***

144

145 Detailed observations of three sections of the Paris chondrite (#2010-1, #2015-L1 and
146 #2015-L2) were made at Centre de Recherches Pétrographique et Géochemique (CRPG) using
147 a scanning electron microscope (SEM) JEOL JSM-6510 equipped with an Energy Dispersive
148 X-ray (EDX) Genesis detector. A 3 nA electron beam accelerated at 15 kV was used for the
149 observations.

150 Quantitative determinations of the chemical composition of carbonates and TCIs
151 (Table S1) were made using a CAMECA SX-100 microprobe (EMPA) at the University of
152 Lorraine (Nancy, France). The analyses were performed with an accelerating voltage of 15
153 kV and a beam current of 12 nA. The microprobe was calibrated using the following natural
154 and synthetic standards: albite for Na and Si, dolomite for Mg, Al₂O₃ for Al, orthoclase

155 feldspar for K, calcite for Ca, barite for S, manganese titanite for Ti and Mn, hematite for Fe,
156 Cr₂O₃ for Cr and NiO for Ni. The detection limits are reported in Table S1.

157

158 *2-2 Raman spectroscopy*

159

160 Raman spectra were obtained using a LabRAM HR spectrometer (Horiba Jobin Yvon)
161 equipped with a 600 gr.mm⁻¹ grating and an Edge filter. The confocal hole aperture and the
162 slit aperture were 500 μm and 100 μm, respectively. The excitation beam was provided by a
163 659.43 nm laser operated at a power of ~20 mW, focused on the sample using a ×100 LWD
164 IR objective (Olympus). The acquisition time and the number of accumulations were chosen
165 in a way as to optimize the signal-to-noise ratio (S/N), usually 10x10s. Calcite and aragonite
166 were identified on the basis of their minor Raman bands; calcite has specific bands at 282 and
167 713 cm⁻¹ while aragonite has bands at 207 and 704 cm⁻¹ (White, 2009). Tochilinite was
168 identified using its unoriented spectra (785nm) from the RUFF database (RUFF ID R060887,
169 Steer and Treiman, 2014). Magnetite was identified using its unoriented spectra (780nm) for
170 the RUFF database (RUFF ID R080025).

171

172 *2-3 Oxygen-isotope measurements*

173

174 Carbonate oxygen isotopic compositions were measured using a CAMECA ims 1280
175 HR2 at CRPG (Nancy, France). ¹⁶O⁻, ¹⁷O⁻, and ¹⁸O⁻ ions produced by a Cs⁺ primary ion beam
176 (15 μm, 5 nA) were measured in multi-collection mode using three Faraday cups. A normal-
177 incidence electron gun was used for charge compensation. In order to remove ¹⁶OH⁻
178 interference on the ¹⁷O⁻ peak and achieve maximum flatness on the top of the ¹⁶O⁻ and ¹⁸O⁻
179 peaks, the entrance and exit slits of the central Faraday cup were adjusted to obtain a Mass

180 Resolving Power ($MRP = M/\Delta M$) of ≈ 7000 for $^{17}\text{O}^-$ on the central Faraday cup. $^{16}\text{O}^-$ and $^{18}\text{O}^-$
181 were measured on L'2 and H1 (slit 1, $MRP \approx 2500$). Acquisition times were set so as to
182 obtain counting statistics on the order of $\pm 0.2 \text{ ‰}$ (1σ) for $\delta^{18}\text{O}$ and $\delta^{17}\text{O}$. We measured two
183 terrestrial standards: (i) quartz from Brazil ($\delta^{18}\text{O} = 9.6 \text{ ‰}$) and (ii) calcite from Mexico ($\delta^{18}\text{O}$
184 $= 23.64 \text{ ‰}$) to define the Terrestrial Fractionation Line (TFL). Isotopes ratios of the Paris Ca-
185 carbonates were normalized to Standard Mean Ocean Water (SMOW). Instrumental Mass
186 Fractionation (IMF) for calcite and aragonite was determined from Mexico calcite, because
187 mineralogical identification of Ca-carbonate grains by Raman spectroscopy was performed
188 after isotopic measurements. The linear deviation of the IMF over the time was also
189 considered by interpolation of its values during time. Typical measurement errors (2σ), which
190 took into account the errors in each measurement as well as the external reproducibility of the
191 standard, were estimated to be $\approx 0.4 \text{ ‰}$ for $\delta^{18}\text{O}$, $\approx 0.6 \text{ ‰}$ for $\delta^{17}\text{O}$, and $\approx 0.4 \text{ ‰}$ for $\Delta^{17}\text{O}$
192 (where $\Delta^{17}\text{O}$ represents the deviation from the TFL: $\Delta^{17}\text{O} = \delta^{17}\text{O} - 0.52 \times \delta^{18}\text{O}$).

193

194 ***2-4 Carbon-isotope measurements***

195 The carbon coat of the sample was removed by polishing its surface with liquid cerium
196 oxide after the SEM, EPMA and O-isotope analyses in order to avoid carbon contamination
197 during the C-isotope measurements. The samples were then coated with gold ($\approx 30 \text{ nm}$) in
198 preparation for carbon isotope analysis using a CAMECA ims 1280 HR2 ion microprobe at
199 CRPG-CNRS (Nancy, France). A Cs^+ primary Gaussian beam of 20 nA was focused to
200 produce a $\approx 20 \text{ }\mu\text{m}$ wide spot. A normal-incidence electron gun was used for charge
201 compensation. The microprobe was specifically tuned to obtain an Mass Resolution Power
202 (MRP) of 5000 so that the $^{12}\text{CH}^-$ contribution to ^{13}C could be eliminated and thus we used the
203 following settings: an $80 \text{ }\mu\text{m}$ entrance slit, a field aperture of $3000 \text{ }\mu\text{m}$, and a $250 \text{ }\mu\text{m}$
204 multicollector slit (slit 2, Rollion-Bard et al., 2007). Carbon isotopes were measured in multi-

205 collection mode using two off-axis faraday cups, C and H1, with 10^{11} ohm resistors for ^{12}C
206 and ^{13}C , respectively. Before each measurement, a presputtering step of 120 s with a raster of
207 $20 \times 20 \mu\text{m}$ was included in the routine analysis in order to remove any remaining traces of
208 the carbon coating. The acquisition times were 5 sec long repeated over 30 cycles and the
209 typical internal error for each measurement was $\approx 0.8\%$ (2σ) on $\delta^{13}\text{C}$. A terrestrial calcite
210 from Mexico ($\delta^{13}\text{C} = -6.37 \%$) was used as a standard to correct for Instrumental Mass
211 Fractionation (IMF) for calcite and aragonite. Isotopes ratios of the Paris Ca-carbonates were
212 normalized to Pee Dee Belemnite (PDB). Typical measurement errors (2σ), which took into
213 account the errors in each measurement as well as the external reproducibility of the standard,
214 were estimated to be $\approx 1.5 \%$.

215

216 **3. Results**

217 ***3.1 Petrographic and mineralogical observations***

218

219 The three sections of Paris examined in this study display heterogeneous degrees of
220 alteration, as marked by significant differences in the abundances of Fe-Ni metal beads and
221 TCIs in the matrix. Relatively fresh zones, rich in Fe-Ni metal ($\approx 3 \%$ of metal), are in direct
222 contact with moderately altered zones that are poor in Fe-Ni metal (only traces of metal,
223 (Hewins et al., 2014). As already described in pervious works, Paris contains abundant Ca-
224 carbonate (hereafter Cc) and TCI alteration products (Marrocchi et al., 2014; Rubin, 2015;
225 Pignatelli et al., 2016, 2017; Vacher et al., 2016). The mineralogical characterization by
226 Raman spectroscopy (Fig. 1a & 1b) reveals that Ca-carbonates are essentially calcite
227 (hereafter C) ($\approx 69 \%$, $n = 29$, Table 1), but a significant proportion of aragonite (hereafter A)
228 was also identified ($\approx 31 \%$, $n = 13$, Table 1). Our petrographic observations highlight that
229 two populations of Ca-carbonates are present. Hereafter, we will follow the classification

230 proposed by Tyra et al. (2012) and Lee et al. (2014). However, we also observed a new type
231 of Ca-carbonate (referred as Type 0) characterized by the absence of TCI and direct contact
232 with the matrix (Fig. 2, see discussion below).

233

234 *3.1.1 Type 1a Ca-carbonate (blue data points)*

235

236 Type 1a Ca-carbonates are dispersed throughout the matrix either in the metal-rich and
237 meta-poor zones (Table 1) and have an average size of a few tens of micrometers. They
238 exhibit varying shapes, with euhedral, subhedral and anhedral crystals all commonly
239 observed, and can occur as single crystal or as complex polycrystalline grains (Fig. 3a to 3d).
240 The Type 1a Ca-carbonates are essentially calcites ($\approx 72\%$, $n = 13$, Table 1) but a few grains
241 of aragonites were also identified ($\approx 28\%$, $n = 5$, Table 1) (Fig. 3a to 3d). All of the Type 1a
242 Ca-carbonates analyzed in the present study are devoid of euhedral Fe-Ni sulphides inclusions
243 and contained significant concentrations of iron (0.9 wt.% Fe on average) (Table S1). A few
244 Ca-carbonate grains also contained: Na₂O (0.2 wt.%, $n = 13$), K₂O (0.3 wt.%, $n = 7$) and S
245 (0.2 wt.%, $n = 12$) (Table S1). Type 1a Ca-carbonates are partially or totally surrounded by
246 tochilinite/cronstedtite rims (TCI) of varying thickness and with irregular sharp to direct
247 contacts with the carbonate grains (Fig. 3a to 3d). The rims are characterized by significant
248 FeO, SiO₂ and S concentrations, with average values of 53.4 wt.%, 14.3 wt.% and 14.3 wt.%,
249 respectively ($n = 34$, Table S1). They were mostly found to be composed of tochilinite (Fig.
250 1c, $n = 11$) but other minerals are also present, such as magnetite (Fig. 4c) as well as other
251 poorly crystalline phases that could not be identified by Raman spectroscopy. The TCI rims
252 are mostly irregular in shape and distorted but some exhibit rectilinear outlines parallel or
253 subparallel to the margin of the central Ca-carbonate grain (Fig. 4a to 4d). The thickness of
254 the TCI rim around a single polycrystalline grain is often variable (Fig. 4a to 4d).

255

256 ***3.1.2 Type 0 Ca-carbonate (green data points)***

257

258 Type 0 Ca-carbonates grains are scattered throughout the matrix either in the fresh and
259 altered areas (Table 1) and have sizes ranging from few tens to few hundreds of micrometers
260 (Fig. 5a to 5d). They present euhedral, subhedral or anhedral shapes and are composed of
261 single or polycrystalline grains. They appear to be inclusion-free. Types 0 are characterized
262 by the absence of TCI rims and direct contact of all the grain/crystal edges with the matrix
263 (Fig. 5a to 5d). Most of the Type 0 Ca-carbonates are calcite ($\approx 77\%$, $n = 16$, Table 1), but a
264 higher proportion of aragonite grains compared to Type 1a ($\approx 33\%$, $n = 8$, Table 1) was
265 identified. The iron content of Type 0 Ca-carbonates is similar to that of Type 1a Ca-
266 carbonates (mean of 0.7 wt.% FeO, $n = 27$, Table S1) and no significant differences in trace-
267 element concentrations were observed between Type 1a and Type 0 Ca-carbonates (Table
268 S1).

269

270 ***3.2 Carbon and oxygen isotopic compositions***

271

272 Carbon and oxygen isotopes were analyzed for both types of Ca-carbonates either in
273 the metal-rich and meta-poor zones. Due to the small sizes of the Ca-carbonates (i.e., a few
274 tens of micrometers in average), we were only able to obtain fourteen C & O isotopic
275 compositions of the same carbonate grain (Table 1).

276

277

278

279

3.2.1 Carbon isotopes

Ca-carbonates show distinct $\delta^{13}\text{C}$ values according to their respective types. Type 1a Ca-carbonates have $\delta^{13}\text{C}$ ranging from 27.3 to 79.7 ‰ with an average value of 48.2 ‰ ($\sigma = 16.9$ ‰, $n = 17$), while $\delta^{13}\text{C}$ values of between 19.1 and 66.2 ‰ were obtained for Type 0 Ca-carbonates (average $\delta^{13}\text{C} = 33.8$ ‰, $\sigma = 13.9$ ‰, $n = 16$) (Fig. 6, Table 1). Type 1a and Type 0 aragonite grains are ^{13}C -rich compared to calcites (55 ‰ vs. 46.1 ‰, respectively, for Type 1a, and 53.2 ‰ vs 27.3 ‰, respectively, for Type 0) (Fig. 6, Table 1).

3.2.2 Oxygen isotopes

In addition to the present data, we also report the oxygen isotopic composition of Ca-carbonates previously measured in Paris (Vacher et al., 2016; notify as *, Table 1). Their mineralogy and petrographic type are also reported (Table 1). Ca-carbonates show specific $\delta^{18}\text{O}$ and $\delta^{17}\text{O}$ values depending on their respective petrographic types. The Type 1a Ca-carbonates have $\delta^{18}\text{O}$ values of between 37.6 and 40.8 ‰ and $\delta^{17}\text{O}$ values of between 19.7 and 20.8 ‰; and they had a mean $\delta^{18}\text{O}$ of 39.4 ‰ ($\sigma = 1.3$ ‰) and mean $\delta^{17}\text{O}$ of 20.4 ‰ ($\sigma = 0.4$ ‰) (Fig. 7, Table 1). The oxygen isotopic compositions of Type 0 Ca-carbonates range from 24.2 to 38.8 ‰ in $\delta^{18}\text{O}$ and from 12.1 to 23.8 ‰ in $\delta^{17}\text{O}$, with average values of 32.5 ‰ ($\sigma = 3.9$ ‰) and 17.1 ‰ ($\sigma = 2.7$ ‰), respectively (Fig. 7, Table 1). Type 1a Ca-carbonates have a narrow range in $\Delta^{17}\text{O}$ of -0.1 ‰ ($\sigma = 0.5$ ‰) whereas significant variations are observed between Type 0 Ca-carbonate grains, with $\Delta^{17}\text{O}$ ranging from -2.5 to 3.6 ‰ (mean $\Delta^{17}\text{O} = 0.2$ ‰, $\sigma = 1.5$ ‰). Type 1a and Type 0 aragonites show slightly higher mean values of $\delta^{18}\text{O}$ and $\delta^{17}\text{O}$ in comparison to Type 1a and Type 0 calcites (37 ‰ in $\delta^{18}\text{O}$ and 19.3 ‰ in $\delta^{17}\text{O}$ vs 31.9 ‰ in $\delta^{18}\text{O}$ and 16.8 ‰ in $\delta^{17}\text{O}$, respectively), but no significant difference in

305 $\Delta^{17}\text{O}$ was observed between aragonite and calcite (except for grain #29*: 3.6 ‰) (Fig. 7,
306 Table 1).

307

308 **4. Discussion**

309

310 *4.1 Relationship between Type 1a Ca-carbonates and TCI rims*

311

312 Petrographic observations of Paris confirm that it contains two types of Ca-carbonates:

313 (i) Type 1a Ca-carbonates surrounded by TCI rims with petrographic characteristics
314 consistent with previous studies of CM carbonaceous chondrites (Tyra et al., 2012; Lee et al.,
315 2014) and (ii) a new Type 0 Ca-carbonates characterized by the absence of TCI rims. Their
316 petrographic features suggest that they likely correspond to two generations of Ca-carbonate
317 precipitation (Brearley, 1998; Lee and Ellen, 2008; Lindgren et al., 2011; Lee et al., 2013,
318 2014; Fujiya et al., 2015; Tyra et al., 2016). In such a scenario, the Type 1a Ca-carbonates
319 would have precipitated at the early stage of alteration, before being partially or totally
320 replaced by TCIs (Fig. 3 and 4). Then, the formation of Type 0 Ca-carbonates could
321 correspond to a late stage of precipitation. However, we do not exclude that the formation of
322 Type 0 Ca-carbonates could also results from an early precipitation in local environments
323 under physicochemical conditions outside the stability field of tochilinite, which forms under
324 restricted conditions characterized by low $f\text{O}_2$, high $f\text{S}_2$ and neutral or alkaline pH (Browning
325 and Bourcier, 1996; Browning et al., 1996; Kozierenko et al., 1996, 2001; Rubin et al., 2007;
326 Pignatelli et al., 2016, 2017).

327 The presence of irregular contacts between Ca-carbonate grains and their TCI rims
328 indicates that Ca-carbonate dissolved during the formation of TCIs. Some of the TCI rims
329 have rectilinear outer edges that are parallel or sub-parallel to the faces of the central

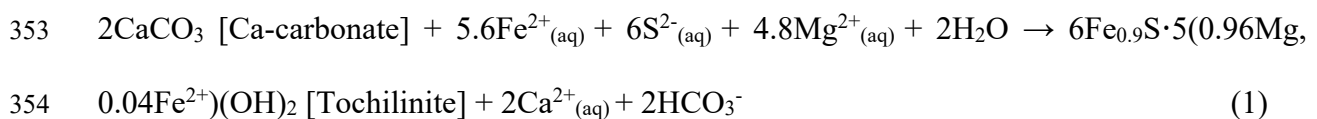
330 carbonate (Fig. 4). This petrographic relationship indicates that the Ca-carbonate precursors
 331 were partially or totally pseudomorphosed by TCIs. Such a process has been previously
 332 reported for the CM 2.2-2.3 carbonaceous chondrite LON 94101, suggesting the ubiquitous
 333 nature of Ca-carbonates as precursors of TCIs (Lee et al., 2013). Interestingly, pseudomorphic
 334 replacement of calcite by serpentine has also been described in terrestrial environments, for
 335 example in magnetite-serpentine-calcite dykes (Robinson, 1975) and in the groundmass of
 336 kimberlite (Clement, 1975). In addition, it has been recently shown that the formation of TCIs
 337 can result from the pseudomorphic replacement of primary high-temperature minerals such as
 338 olivine and pyroxene (Pignatelli et al., 2016). These results imply that the TCIs commonly
 339 observed throughout the CM matrix (Rubin et al., 2007) result from the alteration of different
 340 precursors: (i) anhydrous silicates and (ii) a first generation of Ca-carbonates.

341 In agreement with other studies (Lee et al., 2014; Verdier-Paoletti et al., 2017), our
 342 results demonstrate that the precipitation of Type 1a Ca-carbonates predates the formation of
 343 the TCI. Although thermodynamical calculations suggest that the opposite reaction is also
 344 possible (Browning and Bourcier, 1998), we did not observe any Ca-carbonates surrounding a
 345 tochilinite-cronstedtite core in Paris. We cannot exclude the possibility that the Type 0 Ca-
 346 carbonates might result from complete replacement of TCI grains, but no evidence was found
 347 to support this in Paris. Hence, if Ca-carbonates are the precursors of TCI rims, then two
 348 thermodynamic reactions occurring in different stages of Ca-carbonate alteration can be
 349 distinguished:

350

351 *(i) Precipitation of tochilinite from interactions with Fe, S and Mg-bearing fluids:*

352

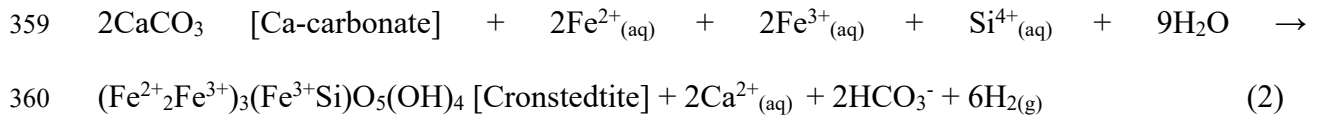


354

355

356 (ii) *Precipitation of cronstedtite from interaction with an Mg- and S-poor and Fe- and*
357 *Si-rich fluid:*

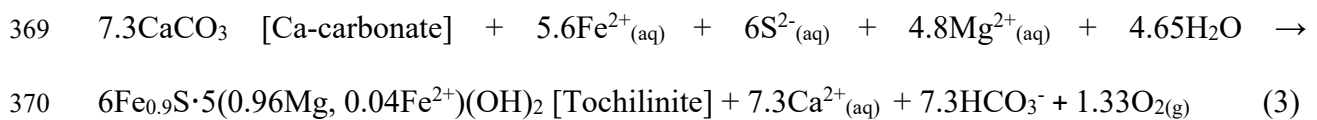
358



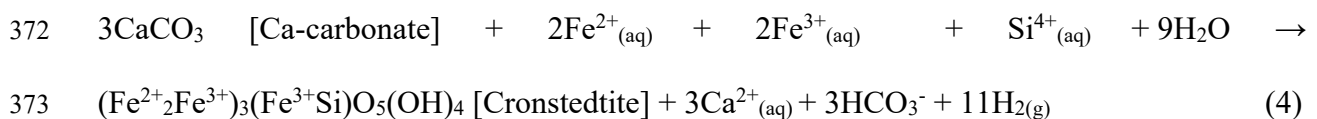
361

362 Similar thermodynamic equations were proposed in other studies (Browning and
363 Bourcier, 1998; Lee et al., 2013). However, as several authors have pointed out (Merino and
364 Dewers, 1998; Hanowski and Brearley, 2001; Pignatelli et al., 2016), pseudomorphic
365 reactions take place at a constant molar volume. Using molar volumes of $\approx 37 \text{ cm}^3 \cdot \text{mol}^{-1}$ for
366 calcite (Ayora, 1999), $\approx 270 \text{ cm}^3 \cdot \text{mol}^{-1}$ for tochilinite (Organova et al., 1972) and ≈ 111
367 $\text{cm}^3 \cdot \text{mol}^{-1}$ for cronstedtite (Helgeson et al., 1978), equations (1) and (2) can be rebalanced:

368



371



374

375 These equations show that tochilinite precipitation requires more than twice the
376 amount of Ca-carbonate than cronstedtite precipitation at a constant molar volume.
377 Consequently, the dissolution of Ca-carbonates would enrich the fluid in Ca^{2+} and C, which
378 could then re-precipitate to form a second generation of Ca-carbonates (Lee et al., 2013). It
379 should be noted that carbonates could also replace ferromagnesian silicates through the

380 introduction of CO₂ from carbonation reactions (Hövelmann et al., 2011; Tyra et al., 2012;
381 Lee et al., 2013). Nevertheless, primary minerals that have been partially replaced by
382 carbonates were not observed in these sections of Paris.

383 The preferential occurrence of tochilinite in the rims of Type 1a Ca-carbonates (Fig.
384 1c) suggests that reaction (3) is dominant in Paris. However, compositional analyses of TCI
385 rims also revealed a high concentration of SiO₂ (i.e., 14.3 wt.%, Table S1), indicating that Fe-
386 rich phyllosilicate phases such as cronstedtite are also present in the rims but it could not be
387 identified by Raman spectroscopy. Furthermore, the fact that the Ca-carbonates are often only
388 partially dissolved by tochilinite suggests that the replacement reactions did not progress to
389 completion. As shown by Pignatelli et al. (2016), cronstedtite coexists with tochilinite under
390 specific conditions, before the cronstedtite becomes progressively more stable as the
391 alteration reaction progresses. Thus, Ca-carbonate dissolution appears to have slowed or
392 ceased at the first stage of the replacement reaction. This interruption could be the result of (i)
393 a change in the alteration conditions (i.e., pH, fluid composition, and/or temperature) and/or
394 (ii) the presence of fluid-limited microenvironments. Several studies also point out that
395 alteration processes probably occur at the micron scale in geochemical microenvironments
396 (Brearley, 2006; Bland et al., 2009; Pignatelli et al., 2016). In Paris, this hypothesis is
397 supported by the presence of several Ca-carbonates grains that have been replaced by TCI in
398 different proportions at scales smaller than 20 µm. For instance, a single grain of Ca-
399 carbonate divided into three parts displays three different stages of replacement (Fig. 4e): (1)
400 initiation of the replacement of the Ca-carbonate (Fig. 4e), (2) near complete replacement
401 (Fig. 4f), and (3) complete replacement of a former Ca-carbonate precursor (Fig. 4e). This
402 observation highlights the heterogeneous nature of the alteration processes that affected CM
403 chondrites, which likely results from their low permeability (Bland et al., 2009) and/or the
404 heterogeneous accretion of sub-micron-sized water ice grains (Lunine, 2006).

4.2 Isotopic compositions of alteration fluids

4.2.1 Sources of carbon

The CM carbonates show a large isotopic variability with their $\delta^{13}\text{C}$ ranging from ≈ 5 to 80 ‰ (this study; Grady et al., 1988; Guo and Eiler, 2007; Alexander et al., 2015; Fujiya et al., 2015; Tyra et al., 2016). Although different C sources and multiple reservoirs with distinct isotopic compositions have been proposed to explain this $\delta^{13}\text{C}$ variability (Grady et al., 1988; Alexander et al., 2015; Fujiya et al., 2015; Tyra et al., 2016), the origin of the C enrichment in carbonates remains disputed. Three potential C sources are generally considered: (i) inorganic carbonaceous ices, (ii) presolar grains and (iii) organic matter (Fig. 8). With regards to the first of these, cometary ices contain several C-bearing inorganic molecules (i.e., CO, CO₂ and CH₄, Cochran et al., 2015), amino acids (i.e., glycine C₂H₅NO₂) and amines (i.e., methylamine CH₅N and ethylamine C₂H₇N) (Altwegg et al., 2016). However, C-bearing molecules measured in 18 comets show an average $\delta^{13}\text{C}$ of -22 ± 39 ‰ (Fig. 8; Manfroid et al., 2009), a value that is significantly lower than the highest $\delta^{13}\text{C}$ measured in the Paris Ca-carbonates. The dissolution of presolar grains could also be responsible for ¹³C-enrichment in CM carbonates (Grady et al., 1988). However, presolar grains (i) show a wide range of $\delta^{13}\text{C}$ with extreme values of up to tens of thousands per mille (Fig. 8; Amari et al., 2014; Davidson et al., 2014), (ii) are present in low abundance (i.e., tens of ppm; Huss and Lewis, 1995) and (iii) show a strong resistance to corrosion by fluids (Amari et al., 1994; Huss and Lewis, 1995). Together, these characteristics make presolar grains an unlikely candidate for the source of the ¹³C-enrichment of altering fluids (Amari et al., 2014; Davidson et al., 2014). Finally, CM carbonaceous chondrites contain substantial amounts of organic matter (up to 4 wt.%), mostly in the form of insoluble organic matter

430 (IOM) (i.e., $\approx 75\%$ of the organic matter; Remusat et al., 2009; Gilmour, 2014; Kuga et al.,
431 2015; Alexander et al., 2017). IOM is mainly located in the chondrite matrices and is
432 composed of highly substituted aromatic moieties linked together by short, highly branched,
433 aliphatic chains (Derenne and Robert, 2010; Le Guillou et al., 2014). CM IOM is ^{13}C -poor,
434 with $\delta^{13}\text{C}$ ranging from ≈ -34 to -8% (Alexander et al., 2007; Alexander et al., 2010) and the
435 Paris' IOM shows the same characteristics with a $\delta^{13}\text{C}$ of -15.8% (Vinogradoff et al., 2015)
436 (Fig. 8). However, the intrinsic insoluble nature of IOM and the range of $\delta^{13}\text{C}$ observed in
437 CM IOMs make unlikely IOM as a direct source of carbon at the origin of CM carbonate
438 precipitation. In contrary, the soluble form of organic matter (SOM), which is present as
439 relatively low molecular weight 'free' compounds, shows a large C-isotopic variability, with
440 $\delta^{13}\text{C}$ ranging from ≈ -15 to 60% (Fig. 8; Sephton, 2002; Gilmour, 2014; Aponte et al., 2016).
441 This range of $\delta^{13}\text{C}$ values is consistent with the C-isotopic compositions of CM carbonates
442 and we therefore suggest that water-soluble organic compounds represent the source of most
443 of the CM carbonates with C isotopic compositions up to 60% . Nevertheless, we noted that
444 SOM could not be involved in the formation of ^{13}C -rich carbonates observed in Paris and in
445 previous studies (i.e., with $\delta^{13}\text{C}$ between 60 and 80%). The C sources responsible for this
446 enrichment is not clearly identified but could be the result of the oxidation or the heating of
447 anomalous IOM with significant $^{17,18}\text{O}$ and ^{13}C enrichments (i.e., $\delta^{17,18}\text{O}$ and $\delta^{13}\text{C}$ up to 530%
448 and 850% , respectively; Hashizume et al., 2011; Fujiya et al., 2015). A contribution of 2 to 4
449 % of anomalous IOM mixed with SOM would thus explain the carbon isotopic compositions
450 of the CM ^{13}C -rich carbonates. However, the behavior of IOM during aqueous alteration
451 processes is still controversial and there are no clear isotopic trend observed during laboratory
452 experiments (Alexander et al., 2017).

453

454

455 **4.2.2 Carbon and oxygen isotopes**

456 **4.2.2.1 Carbon vs oxygen**

457

458 The C and O-isotopic compositions of Paris Ca-carbonates are consistent with those of
459 other CM chondrites (Grady et al., 1988; Guo and Eiler, 2007; Alexander et al., 2015; Fujiya
460 et al., 2015; Tyra et al., 2016). Our data show that Type 1a Ca-carbonates are enriched in ^{13}C
461 and $^{17,18}\text{O}$ compared to Type 0 Ca-carbonates (Table 1), thus confirming the existence of two
462 different populations in Paris, as inferred from petrographic observations (Fig. 3 to 5).
463 Previous studies have also reported these petrographic and isotopic features and proposed that
464 two populations of CM carbonates precipitated under contrasting conditions at different times
465 (Lindgren et al., 2011; Tyra et al., 2012, 2016; Lee et al., 2013, 2014; Fujiya et al., 2015).
466 However, the isotopic evolution of the fluids from which the Ca-carbonates precipitated
467 remains under considerable debate, with both negative and positive $\delta^{13}\text{C}$ - $\delta^{18}\text{O}$ correlations
468 have been reported (Grady et al., 1988; Guo and Eiler, 2007; Tsutsui and Naraoka, 2008,
469 2009; Alexander et al., 2015). Negative correlations were interpreted as a progressive ^{13}C
470 enrichment of the fluid caused by the release of ^{12}C -enriched CH_4 during carbonate
471 precipitation (Guo and Eiler, 2007), whereas positive correlations are understood in terms of
472 carbonate precipitation from the evolution of a single fluid in equilibrium with water and C-
473 bearing gases (i.e., CO , CH_4 and potentially CO_2) at temperatures in the range 0-130°C (Yuen
474 et al., 1984; Alexander et al., 2015). In first approximation, the C and O-isotopic
475 compositions of the Paris Ca-carbonates define a positive $\delta^{13}\text{C}$ - $\delta^{18}\text{O}$ trend with general
476 relationship of $\delta^{13}\text{C} = (5.0 \pm 1.8) \times \delta^{18}\text{O} - (128 \pm 65)$ (2σ , $R^2 = 0.71$, $n = 14$; Fig. 9). However,
477 the mean square weighted deviation (MSWD) is relatively high (115) and we rather interpret
478 our data as two different carbonate populations with varying $\delta^{13}\text{C}$ - $\delta^{18}\text{O}$. These C and O-
479 isotopic ranges can be approximately reproduced by the equilibration of a CO - or CH_4 -

480 dominated gas ($\delta^{13}\text{C}_{\text{CO}} = -33 \text{ ‰}$ and $\delta^{13}\text{C}_{\text{CH}_4} = -20 \text{ ‰}$) with a $\delta^{18}\text{O}$ -poor aqueous fluid ($\delta^{18}\text{O} =$
481 5 ‰) at different temperatures (Fig. 10, Alexander et al., 2015). However, this model assumes
482 that the O-isotopic composition of the initial alteration fluid is $\delta^{18}\text{O} \approx 5 \text{ ‰}$ (Alexander et al.,
483 2015). Because Paris is the least altered CM chondrite (Hewins et al., 2014; Marrocchi et al.,
484 2014), this value appears unlikely and the Paris' water should $^{17,18}\text{O}$ -rich compared to the
485 other CM chondrites (Clayton and Mayeda, 1984, 1999; Verdier-Paoletti et al., 2017). In
486 addition, such a model requires infinite C and O fluid reservoirs. This seems unlikely
487 regarding the partial pseudomorphism of Ca-carbonates by TCIs that indicates fluid-limited
488 geochemical microenvironments.

489 Here, we develop an alternative model that considers that the Paris Ca-carbonates
490 precipitated from different fluids derived from (i) variable equilibration of $^{17,18}\text{O}$ -rich
491 primordial water (hereafter PW) with ^{16}O -rich matrix anhydrous silicates and (ii) variable
492 contributions of different ^{12}C - and ^{13}C -rich SOMs. The O-isotopic composition of CM
493 carbonates follows a continuous trend that crosses the mass-dependent fractionation line (Fig.
494 7; Hortsman et al., 2014; Verdier-Paoletti et al., 2017). This implies that the O-isotopic
495 composition of Ca-carbonates did not result from fluid circulation along a temperature
496 gradient but rather recorded varying isotopic equilibration between a $^{17,18}\text{O}$ -rich fluid (i.e.,
497 $\delta^{18}\text{O} \approx 30.3 \text{ ‰}$, $\delta^{17}\text{O} \approx 20.2 \text{ ‰}$, Clayton and Mayeda, 1984) and ^{16}O -rich anhydrous silicates
498 i.e., $\delta^{18}\text{O} \approx -4.2 \text{ ‰}$, $\delta^{17}\text{O} \approx -7.4 \text{ ‰}$, Clayton and Mayeda, 1984). Interestingly, the O-isotopic
499 compositions of water extracted from different CM chondrites also define a linear relationship
500 (the CM water line; hereafter CMW) with a similar slope that the carbonate trend but with a
501 different intercept (Clayton and Mayeda, 1984, 1999; Verdier-Paoletti et al., 2017). The
502 distance between the carbonate trend and the CMW line simply reflect the fractionation factor
503 α , which is directly related to the temperature of precipitation (Verdier-Paoletti et al., 2017).
504 Consequently, the $^{17,18}\text{O}$ -rich CM carbonates result from the precipitation of a fluid that is less

505 equilibrated with ^{16}O -rich anhydrous silicates than the $^{17,18}\text{O}$ -poor carbonates (Tyra et al.,
506 2012; Lee et al., 2013; Verdier-Paoletti et al., 2017; Lindgren et al., 2017). This also implies
507 that the $\delta^{18}\text{O}$ of the fluids from which Ca-carbonates precipitated can only be located within a
508 range of values between -4.2 ‰ and 30.2 ‰ (Fig. 11a), which correspond to the values of the
509 starting anhydrous silicates and the primordial water (PW; Fig. 11a), respectively.

510 The $^{17,18}\text{O}$ -rich Ca-carbonates are also enriched in ^{13}C (Fig. 9), with the heaviest
511 carbonates showing a $\delta^{13}\text{C}$ of ≈ 80 ‰. To the contrary, the ^{16}O -rich Ca-carbonates present
512 lower $\delta^{13}\text{C}$ values in the range 20 to 40 ‰ (Fig. 9, Table 1). As detailed above (see paragraph
513 4.2.1), these extreme $\delta^{13}\text{C}$ values could correspond to the respective contribution of different
514 types of SOMs characterized by ^{12}C - and ^{13}C - enrichments, respectively (Fig. 11a). This
515 suggest that the fluids at the origin of Ca-carbonates can only be located in a specific area of
516 the $\delta^{13}\text{C}$ - $\delta^{18}\text{O}$ diagram delineated by (i) the extreme $\delta^{13}\text{C}$ values measured in the different
517 SOMs (Fig. 11a) and (ii) the $\delta^{18}\text{O}$ of the primordial water and the anhydrous CM silicates
518 (Fig. 11a). Taking into account that the low fractionation factor between Ca-carbonate and
519 carbonate ion in the fluids over a large temperature range (i.e., $1000\ln \alpha_{\text{CaCO}_3\text{-HCO}_3^-} = 2.2$ ‰ at
520 0°C and 1.2 ‰ at 300°C , Deines et al., 1974; Luo and Wang, 2009) as well as the important
521 fractionation factor of oxygen isotopes between the fluid and the precipitated carbonates (Kim
522 and O'Neil, 1997), the final $\delta^{13}\text{C}$ - $\delta^{18}\text{O}$ compositions of Ca-carbonates are shifted to the right
523 of the $\delta^{13}\text{C}$ - $\delta^{18}\text{O}$ diagram with an intensity that is a function of the precipitation temperature
524 (Fig. 11b). Assuming that the average precipitation temperatures of CM Ca-carbonates is \approx
525 110°C (Verdier-Paoletti et al., 2017), the possible $\delta^{13}\text{C}$ - $\delta^{18}\text{O}$ carbonate values estimated by
526 this model (Fig. 11b) are consistent with those reported here and in previous *in situ* studies
527 (Fujiya et al., 2015; Tyra et al., 2016).

528 According to the degree of equilibration between the PW and the anhydrous silicates
529 (f), the $\delta^{18}\text{O}$ of the alteration fluids can be calculated using the following isotopic mass
530 balance equations:

$$531 \quad \delta^{18}\text{O}_{\text{fluid}} = f \times \delta^{18}\text{O}_{\text{anhydrous silicates}} + (1 - f) \times \delta^{18}\text{O}_{\text{PW}} \quad (5)$$

532
533 The equation (5) assumes that (i) the O-isotopic composition of the fluid is essentially
534 controlled by the equilibration between the fluid and the anhydrous silicates and (ii) there is
535 no influence of the phyllosilicate formation on the O-isotopic composition of the alteration
536 fluid. The latter assumption is consistent with the lower average temperature formation of
537 phyllosilicates comparing to Ca-Carbonates in CM chondrites (i.e., 75°C vs. 110°C; Verdier-
538 Paoletti et al., 2017). In addition, considering the volume of TCI in Paris (12 ± 3%; Rubin,
539 2015) and a fractional precipitation process for phyllosilicates ($1000 \ln \alpha_{\text{serp-H}_2\text{O}} = 8.2$ at 75°C,
540 Wenner and Taylor, 1971, the $\delta^{18}\text{O}$ of the fluid would decrease by only 1 - 2 ‰ at 75°C for a
541 serpentine precipitation rate of 15% ($\delta_{\text{water}} = 1000 \times (0.85^{\alpha-1} - 1) + \delta_{\text{PW}}$).

542 Our model demonstrates that the *in situ* variability in the C and O-isotopic
543 compositions of Paris Ca-carbonates can be explained by precipitation events occurring at
544 different temperatures from alteration fluids characterized by varying (i) degrees of O-
545 isotopic equilibration between PW and the matrix and (ii) contributions of ^{12}C - and ^{13}C -rich
546 SOMs. It appears that —depending on the degree of alteration and the respective contribution
547 of the different types of SOMs—both positive and negative $\delta^{13}\text{C}$ - $\delta^{18}\text{O}$ correlations can be
548 produced during the precipitation of Ca-carbonates (Fig. 11). However, given that Ca-
549 carbonate precipitation can occur at variable temperatures, from fluids characterized by
550 different degrees of equilibration and with variable ^{12}C and ^{13}C -rich SOMs, we consider it is
551 more likely that no systematic relationship between $\delta^{13}\text{C}$ and $\delta^{18}\text{O}$ should be observed in CM
552 chondrites, as previously reported from *in situ* analysis (Fujiya et al., 2015; Tyra et al., 2016).

553

554 *4.2.3 Aragonite vs calcite*

555

556 A significant proportion of the Type 1a or Type 0 Ca-carbonates in Paris were
557 identified to be aragonite, as was also the case in other poorly altered CM chondrites (Fig 2,
558 Barber, 1981; Lee and Ellen, 2008; Sofe, 2013; Lee et al., 2013, 2014). Both types of
559 aragonite are ¹³C- and ^{17,18}O-rich relative to the Type 1a and Type 0 calcites (Fig. 6 & 7,
560 Table 1). From petrographic observations, previous studies have suggested that (i) aragonite
561 precipitated after calcite in Cold Bokkeveld and Murray (Barber, 1981; Lee and Ellen, 2008)
562 and (ii) that aragonite predates calcite in the least altered CM chondrites (Lee et al., 2013,
563 2014). Because aragonites can occur as both Type 1a and Type 0 Ca-carbonates in Paris, our
564 petrographic observations do not allow the sequence of Ca-carbonate precipitation to be better
565 constrained. However, the O-isotopic compositions of the aragonites are ^{17,18}O-rich relative to
566 the calcites, suggesting early precipitation from an ¹⁸O-rich fluid that had not experienced
567 protracted O-isotopic equilibration with the matrix anhydrous silicates.

568 Thermodynamic calculations predict that calcite is stable under the conditions under
569 which aqueous alteration of the CM-chondrite parent bodies occurred (Zolensky et al., 1993),
570 while Ostwald's rule predicts that the least stable polymorph (i.e., aragonite for CaCO₃) would
571 crystallize first (Van Santen, 1984). Furthermore, several factors favor the precipitation of
572 aragonite over calcite: (i) the presence of dissolved organic carbon (DOC), Mg²⁺, Fe²⁺ and
573 SO₄²⁻ in solution (Berner, 1975; Meyer, 1984; Walter, 1986; Lebron and Suarez, 1996), (ii) a
574 high precipitation rate (Given and Wilkinson, 1985), and (iii) a high temperature (Walter,
575 1986). Recently, Lee et al. (2014) proposed that CM aragonite precipitated from Mg-rich
576 solutions during brief precipitation events and/or under low water/rock ratios. In addition,
577 aragonite precipitation is expected to occur when (i) the fluid Mg/Ca ratio is constant and the

578 temperature increases or (ii) when the temperature is constant and the fluid Mg/Ca ratio
579 increases (Morse et al., 1997). Hence, the precipitation of aragonite in Paris could have
580 resulted from an increase in the temperature or from an increase in the Mg²⁺ concentration in
581 the fluid caused by the dissolution of mafic silicate (Lee and Ellen, 2008; Leroux et al., 2015;
582 Pignatelli et al., 2016). A decrease in the Mg/Ca ratio caused by either the precipitation of
583 TCI or the dissolution of Type 1a aragonite would have enriched the fluid in Ca²⁺, leading to
584 the precipitation of calcite that postdate aragonite. However, the presence of euhedral crystals
585 of aragonite (Fig. 3a) indicates that this dissolution of Type 1a aragonite in Paris is selective
586 with the increase of aqueous alteration, confirming the presence of fluid-limited
587 microenvironments. We thus propose that aragonite represents the first Ca-carbonate that
588 precipitated only during the earliest stage of fluid alteration of CM chondrites.

589

590 **5. Conclusions**

591

592 Our petrographic and isotopic study of Ca-carbonates in the least altered CM Paris has
593 offered us a unique opportunity to better characterize the early stages of aqueous alteration in
594 the CM parent body. Our results have revealed different alteration histories and have allowed
595 us to place new constraints on the physicochemical conditions under which the alteration of
596 CM chondrites took place.

597 (1) Two populations of Ca-carbonates are found in Paris. Type 1a refers to grains that are
598 surrounded by TCIs (identified to be mainly tochilinite) whereas new Type 0 Ca-
599 carbonates refer to isolated TCI-free grains. Petrographic observations suggest that
600 Type 1a Ca-carbonates precipitated at the earliest stages of alteration, before the
601 precipitation of Type 0 Ca-carbonates.

- 602 (2) TCI rims commonly have rectilinear shapes with planar margins that are parallels or
603 subparallels to the central carbonate grain. Individual Ca-carbonate grains can display
604 contrasting degrees of alteration with partial or complete replacement by TCIs. These
605 features suggest that Type 1a Ca-carbonates were pseudomorphosed by TCIs at the
606 micron scale within geochemical microenvironments.
- 607 (3) Few Type 1a and Type 0 Ca-carbonates were identified as aragonites. The aragonites
608 were found to be ^{13}C and $^{17,18}\text{O}$ -rich relative to the calcites, suggesting early
609 precipitation from a fluid that had not undergone protracted isotopic exchange with
610 the matrix.
- 611 (4) Based on recent reports of the C-isotopic composition of low molecular weight 'free'
612 compounds in CM chondrites, we propose that water-soluble organic compounds
613 (SOM) represent the major source of the ^{13}C -rich carbonates.
- 614 (5) We developed a model in which the C and O isotopic composition of Ca-carbonates
615 results from varying (i) equilibration $^{17,18}\text{O}$ -rich primordial water with ^{16}O -rich
616 anhydrous silicates and (ii) contributions of ^{12}C - and ^{13}C -rich soluble organic matter.
- 617 (6) Our model suggests that CM Ca-carbonates can record both positive and negative
618 $\delta^{13}\text{C}$ - $\delta^{18}\text{O}$ correlations. However, given that Ca-carbonates precipitation can occur at
619 variable temperature from a fluid with different degrees of equilibration and variable
620 ^{12}C and ^{13}C -rich SOMs, there is probably no systematic relationship between $\delta^{13}\text{C}$
621 and $\delta^{18}\text{O}$ in CM carbonates.

622

623 **Acknowledgments**

624

625 We are grateful to Nordine Bouden for his assistance with the oxygen and carbon
626 isotope measurements and to Marie-Camille Caumon for her assistance with the Raman

627 analyses. This work was funded by l'Agence Nationale de la Recherche through grant ANR-
628 14-CE33-0002-01 SAPINS (PI Yves Marrocchi). We thanked Wataru Fujiya, Martin R. Lee
629 and an anonymous reviewer for constructive comments and Associate Editor Sara Russell for
630 careful editing. This is CRPG contribution #2473 and SAPINS contribution #08.

631

632 **References**

633

634 Alexander C. M. O., Fogel M., Yabuta H. and Cody G. D. (2007) The origin and evolution of
635 chondrites recorded in the elemental and isotopic compositions of their
636 macromolecular organic matter. *Geochim. Cosmochim. Acta* **71**, 4380–4403.

637 Alexander C. M. O., Newsome S. D., Fogel M. L., Nittler L. R., Busemann H. and Cody G.
638 D. (2010) Deuterium enrichments in chondritic macromolecular material—
639 Implications for the origin and evolution of organics, water and asteroids. *Geochim.*
640 *Cosmochim. Acta* **74**, 4417–4437.

641 Alexander C. M. O., Bowden R., Fogel M. L., Howard K. T., Herd C. D. K. and Nittler L. R.
642 (2012) The Provenances of Asteroids, and Their Contributions to the Volatile
643 Inventories of the Terrestrial Planets. *Science* **337**, 721–723.

644 Alexander C. M. O., Bowden R., Fogel M. L. and Howard K. T. (2015) Carbonate
645 abundances and isotopic compositions in chondrites. *Meteorit. Planet. Sci.* **50**, 810–
646 833.

647 Alexander C. M. O., Cody G. D., De Gregorio B. T., Nittler L. R. and Stroud R. M. (2017)
648 The nature, origin and modification of insoluble organic matter in chondrites, the
649 major source of Earth's C and N. *Chem. Erde - Geochem.*

650 Altwegg, K., Balsiger H., Bar-Nun A., Berthelier J.-J., Bieler A., Bochsler P., Briois C., et al.
651 (2016) Prebiotic Chemicals—amino Acid and Phosphorus—in the Coma of Comet
652 67P/Churyumov-Gerasimenko.” *Sci. Adv.* **2**, no. 5.

653 Amari S., Zinner E. and Gallino R. (2014) Presolar graphite from the Murchison meteorite:
654 An isotopic study. *Geochim. Cosmochim. Acta* **133**, 479–522.

655 Aponte J. C., McLain H. L., Dworkin J. P. and Elsila J. E. (2016) Aliphatic amines in
656 Antarctic CR2, CM2, and CM1/2 carbonaceous chondrites. *Geochim. Cosmochim.*
657 *Acta* **189**, 296–311.

658 Ayora, C. (1999) Modelo de dedolomitización. In: Armenteros, I., Blanco Sánchez, J.A.,
659 Merino E., (Eds), Dinámica de las interacciones entre agua y minerales en medios de
660 baja temperatura (meteorización, diagénesis, metasomatismo). Reunion Científica y
661 Curso Extraordinario, Salamanca, pp. 197-207.

662 Barber D. J. (1981) Matrix phyllosilicates and associated minerals in C2M carbonaceous

- 663 chondrites. *Geochim. Cosmochim. Acta* **45**, 945–970.
- 664 Benedix G. ., Leshin L. ., Farquhar J., Jackson T. and Thiemens M. . (2003) Carbonates in
665 CM2 chondrites: constraints on alteration conditions from oxygen isotopic
666 compositions and petrographic observations. *Geochim. Cosmochim. Acta* **67**, 1577–
667 1588.
- 668 Berner R. A. (1975) The role of magnesium in the crystal growth of calcite and aragonite
669 from sea water. *Geochim. Cosmochim. Acta* **39**, 489–504.
- 670 Bland P. A., Jackson M. D., Coker R. F., Cohen B. A., Webber J. B. W., Lee M. R., Duffy C.
671 M., Chater R. J., Ardakani M. G., McPhail D. S., McComb D. W. and Benedix G. K.
672 (2009) Why aqueous alteration in asteroids was isochemical: High porosity≠high
673 permeability. *Earth Planet. Sci. Lett.* **287**, 559–568.
- 674 Boss A. P. and Goswami J. N. (2006) Presolar cloud collapse and the formation and early
675 evolution of the solar nebula. *Meteor. Early Sol. Syst. II*, 171–186.
- 676 Bourot-Denise M., Zanda B., Marrocchi Y., Greenwood R. C., Pont S., Hewins R. H., Franchi
677 I. A. and Cornen G. (2010) Paris: The slightly altered, slightly metamorphosed CM
678 that bridges the gap between CMs and COs. *Lunar Planet. Sci. 41*. Lunar Planet. Inst.,
679 Houston. #1683 (abstr.).
- 680 Brearley A. J. (1998) Carbonates in CM Carbonaceous Chondrites: Complex Zoning
681 Revealed by High Resolution Cathodoluminescence Studies. In *Lunar and Planetary
682 Science Conference* Lunar and Planetary Inst. Technical Report.
- 683 Brearley A. J. (2006) The action of water. *Meteor. Early Sol. Syst. II* **943**, 587–624.
- 684 Browning L. B., McSween H. Y. and Zolensky M. E. (1996) Correlated alteration effects in
685 CM carbonaceous chondrites. *Geochim. Cosmochim. Acta* **60**, 2621–2633.
- 686 Browning L. B. and Bourcier W. L. (1998) On the Origin of Rim Textures Surrounding
687 Carbonate Grains in CM Matrices. *Lunar Planet. Sci. 29*. Lunar Planet. Inst., Houston.
688 #1533 (abstr.).
- 689 Ciesla F. J. and Scott A. (2012) Organic Synthesis via Irradiation and Warming of Ice Grains
690 in the Solar Nebula. *Science* **336**, 452–454.
- 691 Clayton R. N. and Mayeda T. K. (1984) The oxygen isotope record in Murchison and other
692 carbonaceous chondrites. *Earth Planet. Sci. Lett.* **67**, 151–161.
- 693 Clayton R. N. and Mayeda T. K. (1999) Oxygen isotope studies of carbonaceous chondrites.
694 *Geochim. Cosmochim. Acta* **63**, 2089–2104.
- 695 Clement C. R. (1975) The emplacement of some diatrema-facies kimberlites. *Phys. Chem.
696 Earth* **9**, 51–59.
- 697 Cochran A. L., Levasseur-Regourd A.-C., Cordiner M., Hadamcik E., Lasue J., Gicquel A.,
698 Schleicher D. G., Charnley S. B., Mumma M. J., Paganini L., Bockelée-Morvan D.,
699 Biver N. and Kuan Y.-J. (2015) The Composition of Comets. *Space Sci. Rev.* **197**, 9–
700 46.

- 701 Cohen B. A. and Coker R. F. (2000) Modeling of Liquid Water on CM Meteorite Parent
702 Bodies and Implications for Amino Acid Racemization. *Icarus* **145**, 369–381.
- 703 Coker R. and Cohen B. (2001) The effect of liquid transport on the modeling of CM parent
704 bodies. *Meteorit. Planet. Sci. Suppl.* **36**, 43.
- 705 Connelly J. N., Bizzarro M., Krot A. N., Nordlund Å., Wielandt D. and Ivanova M. A. (2012)
706 The Absolute Chronology and Thermal Processing of Solids in the Solar
707 Protoplanetary Disk. *Science* **338**, 651.
- 708 Davidson J., Busemann H., Nittler L. R., Alexander C. M. O., Orthous-Daunay F.-R., Franchi
709 I. A. and Hoppe P. (2014) Abundances of presolar silicon carbide grains in primitive
710 meteorites determined by NanoSIMS. *Geochim. Cosmochim. Acta* **139**, 248–266.
- 711 De Leuw S., Rubin A. E. and Wasson J. T. (2010) Carbonates in CM chondrites: Complex
712 formational histories and comparison to carbonates in CI chondrites: Carbonates in
713 CM chondrites. *Meteorit. Planet. Sci.* **45**, 513–530.
- 714 Deines P., Langmuir D. and Harmon R. S. (1974) Stable carbon isotope ratios and the
715 existence of a gas phase in the evolution of carbonate ground waters. *Geochim.*
716 *Cosmochim. Acta* **38**, 1147–1164.
- 717 Derenne S. and Robert F. (2010) Model of molecular structure of the insoluble organic matter
718 isolated from Murchison meteorite. *Meteorit. Planet. Sci.* **45**, 1461–1475.
- 719 Doyle P. M., Jogo K., Nagashima K., Krot A. N., Wakita S., Ciesla F. J. and Hutcheon I. D.
720 (2015) Early aqueous activity on the ordinary and carbonaceous chondrite parent
721 bodies recorded by fayalite. *Nat. Commun.* **6**, 7444.
- 722 Dyl K. A., Bischoff A., Ziegler K., Young E. D., Wimmer K. and Bland P. A. (2012) Early
723 Solar System hydrothermal activity in chondritic asteroids on 1-10-year timescales.
724 *Proc. Natl. Acad. Sci. U. S. A.* **109**, 18306–18311.
- 725 Fujiya W., Sugiura N., Marrocchi Y., Takahata N., Hoppe P., Shirai K., Sano Y. and Hiyagon
726 H. (2015) Comprehensive study of carbon and oxygen isotopic compositions, trace
727 element abundances, and cathodoluminescence intensities of calcite in the Murchison
728 CM chondrite. *Geochim. Cosmochim. Acta* **161**, 101–117.
- 729 Gilmour I. (2014) Structural and isotopic analysis of organic matter in carbonaceous
730 chondrites. In *Treatise on Geochemistry*. Elsevier, 215-233.
- 731 Given R. K. and Wilkinson B. H. (1985) Kinetic control of morphology, composition, and
732 mineralogy of abiogenic sedimentary carbonates. *J. Sediment. Res.* **55**, 109.
- 733 Grady M. M., Wright I. ., Swart P. . and Pillinger C. . (1988) The carbon and oxygen isotopic
734 composition of meteoritic carbonates. *Geochim. Cosmochim. Acta* **52**, 2855–2866.
- 735 Grimm R. (2007) Fluid flow on carbonaceous chondrite parent bodies. *Lunar Planet. Sci.* **38**.
736 Lunar Planet. Inst., Houston. #1327 (abstr.).
- 737 Grimm R. E. and Mccween H. Y. (1989) Water and the thermal evolution of carbonaceous
738 chondrite parent bodies. *Icarus* **82**, 244–280.

- 739 Grossman J. N. and Alexander C. M. O. (2004) Entry of alkalis into type-I chondrules at both
740 high and low temperatures. *Meteorit. Planet. Sci.* **39**.
- 741 Grossman J. N., Alexander C. M. O., Wang J. and Brearley A. J. (2000) Bleached chondrules:
742 Evidence for widespread aqueous processes on the parent asteroids of ordinary
743 chondrites. *Meteorit. Planet. Sci.* **35**, 467–486.
- 744 Grossman J. N., Alexanders C. M. O., Wang J. and Brearley A. J. (2002) Zoned chondrules in
745 Semarkona: Evidence for high- and low-temperature processing. *Meteorit. Planet. Sci.*
746 **37**, 49–73.
- 747 Guo W. and Eiler J. M. (2007) Temperatures of aqueous alteration and evidence for methane
748 generation on the parent bodies of the CM chondrites. *Geochim. Cosmochim. Acta* **71**,
749 5565–5575.
- 750 Hanowski N. P. and Brearley A. J. (2001) Aqueous alteration of chondrules in the CM
751 carbonaceous chondrite, Allan Hills 81002: implications for parent body alteration.
752 *Geochim. Cosmochim. Acta* **65**, 495–518.
- 753
- 754 Hashizume K., Takahata N., Naraoka H. and Sano Y. (2011) Extreme Oxygen Isotope
755 Anomaly with a Solar Origin Detected in Meteoritic Organics. *Nat. Geosci* **4**, 165-
756 168.
- 757 Helgeson H. C., Delany J. M. and Nesbitt H. W. (1978) *Summary and critique of the*
758 *thermodynamic properties of rock - forming minerals.*, Yale Univ., New Haven
759 (Conn.).
- 760 Hewins R. H., Bourot-Denise M., Zanda B., Leroux H., Barrat J.-A., Humayun M., Göpel C.,
761 Greenwood R. C., Franchi I. A., Pont S., Lorand J.-P., Cournède C., Gattacceca J.,
762 Rochette P., Kuga M., Marrocchi Y. and Marty B. (2014) The Paris meteorite, the
763 least altered CM chondrite so far. *Geochim. Cosmochim. Acta* **124**, 190–222.
- 764 Horstmann M., Vollmer C., Birth M. I. F., Chaussidon M., Gurenko A. and Bischoff A.
765 (2014) Tracking aqueous alteration of CM chondrites—Insight from in-situ oxygen
766 isotope measurements of calcite. *Lunar Planet. Sci.* 45. Lunar Planet. Inst., Houston.
767 #1761 (abstr.).
- 768 Hövelmann J., Austrheim H., Beinlich A. and Anne Munz I. (2011) Experimental study of the
769 carbonation of partially serpentinized and weathered peridotites. *Geochim.*
770 *Cosmochim. Acta* **75**, 6760–6779.
- 771 Huss G. R. and Lewis R. S. (1995) Presolar diamond, SiC, and graphite in primitive
772 chondrites: Abundances as a function of meteorite class and petrologic type. *Geochim.*
773 *Cosmochim. Acta* **59**, 115–160.
- 774 Johansen A., Jacquet E., Cuzzi J. N., Morbidelli A. and Gounelle M. (2015) New paradigms
775 for asteroid formation. *Asteroids IV*, 471–492.
- 776 Kerridge, J. F., Mackay, A. J. and Boynton, W. V. (1979) Magnetite in CI Carbonaceous
777 Meteorites: Origin by Aqueous Activity on a Planetesimal Surface. *Science* 205, no.
778 4404 (July 27, 1979): 395.

- 779 Kim S.-T. and O'Neil J. R. (1997) Equilibrium and nonequilibrium oxygen isotope effects in
780 synthetic carbonates. *Geochim. Cosmochim. Acta* **61**, 3461–3475.
- 781 Kozerenko S.V., Fadeev V.V., Organova N.I., Chstyakova N.I., Kolpakova N.N. and Senin V.G.
782 (2001) Synthesis, formation conditions and crystallochemistry of tochilinites – iron,
783 magnesium and sodium hydroxide-sulfides. *Experiment in Geosciences* **10**, 57-58.
- 784 Kozerenko S.V., Organova N.J., Fadeev V.V., Magazina L.O., Kolpakova N.N. and Kopneva
785 L.A. (1996) Tochilinite produced in laboratory. *Lunar Planet. Sci. XXVII*. Lunar Planet.
786 Inst., Houston. 695-696 (abstr.).
- 787 Kuga M., Marty B., Marrocchi Y. and Tissandier L. (2015) Synthesis of refractory organic
788 matter in the ionized gas phase of the solar nebula. *Proc. Natl. Acad. Sci.* **112**, 7129–
789 7134.
- 790 Le Guillou C., Bernard S, Brearley A. J. and Remusat L. (2014) Evolution of Organic Matter
791 in Orgueil, Murchison and Renazzo during Parent Body Aqueous Alteration: In Situ
792 Investigations. *Geochim. Cosmochim. Acta* **131**, 368–392.
- 793 Le Guillou C., Changela H. and Brearley A. (2015) Ubiquitous Oxidized and Hydrated
794 Amorphous Silicates in Carbonaceous and Ordinary Chondrites: Implications for
795 Alteration Conditions and H₂ Degassing of Asteroids. *Lunar Planet. Sci. 46*. Lunar
796 Planet. Inst., Houston. #2599 (abstr.).
- 797 Lebron I. and Suarez D. L. (1996) Calcite nucleation and precipitation kinetics as affected by
798 dissolved organic matter at 25°C and pH > 7.5. *Geochim. Cosmochim. Acta* **60**, 2765–
799 2776.
- 800 Lee M. R. and Ellen R. (2008) Aragonite in the Murray (CM2) carbonaceous chondrite:
801 implications for parent body compaction and aqueous alteration. *Meteorit. Planet. Sci.*
802 **43**, 1219–1231.
- 803 Lee M. R., Sofe M. R., Lindgren P., Starkey N. A. and Franchi I. A. (2013) The oxygen
804 isotope evolution of parent body aqueous solutions as recorded by multiple carbonate
805 generations in the Lonewolf Nunataks 94101 CM2 carbonaceous chondrite. *Geochim.*
806 *Cosmochim. Acta* **121**, 452–466.
- 807 Lee M. R., Lindgren P. and Sofe M. R. (2014) Aragonite, breunnerite, calcite and dolomite in
808 the CM carbonaceous chondrites: High fidelity recorders of progressive parent body
809 aqueous alteration. *Geochim. Cosmochim. Acta* **144**, 126–156.
- 810 Leroux H., Cuvillier P., Zanda B. and Hewins R. H. (2015) GEMS-like material in the matrix
811 of the Paris meteorite and the early stages of alteration of CM chondrites. *Geochim.*
812 *Cosmochim. Acta* **170**, 247–265.
- 813 Lindgren P., Lee M. R., Sofe M. and Burchell M. J. (2011) Microstructure of calcite in the
814 CM2 carbonaceous chondrite LON 94101: Implications for deformation history
815 during and/or after aqueous alteration. *Earth Planet. Sci. Lett.* **306**, 289–298.
- 816 Lindgren P., Lee M.R., Starkey N. A. and Franchi I. A. (2017) Fluid evolution in CM
817 carbonaceous chondrites tracked through the oxygen isotopic compositions of
818 carbonates. *Geochim. Cosmochim. Acta* **204**, 240–251.

- 819 Lunine J. I. (2006) Origin of water ice in the solar system. *Meteor. Early Sol. Syst. II* **1**, 309–
820 319.
- 821 Luo W. and Wang S. (2009) Transmission of $\delta^{13}\text{C}$ signals and its paleoclimatic implications
822 in Liangfeng Cave system of Guizhou Province, SW China. *Environ. Earth Sci.* **59**,
823 655–661.
- 824 Manfroid J., Jehin E., Hutsemékers D., Cochran A., Zucconi J.-M., Arpigny C., Schulz R.,
825 Stüwe J. A. and Ilyin I. (2009) The CN isotopic ratios in comets. *Astron. Astrophys.*
826 **503**, 613–624.
- 827 Marrocchi Y., Gounelle M., Blanchard I., Caste F. and Kearsley A. T. (2014) The Paris CM
828 chondrite: Secondary minerals and asteroidal processing. *Meteorit. Planet. Sci.* **49**,
829 1232–1249.
- 830 McSween H. Y. (1979) Are carbonaceous chondrites primitive or processed? A review. *Rev.*
831 *Geophys.* **17**, 1059–1078.
- 832 McSween Jr H. Y., Ghosh A., Grimm R. E., Wilson L. and Young E. D. (2002) Thermal
833 evolution models of asteroids. *Asteroids III* **559**.
- 834 Merino E. and Dewers T. (1998) Implications of replacement for reaction–transport modeling.
835 *J. Hydrol.* **209**, 137–146.
- 836 Metzler K., Bischoff A. and Stöffler D. (1992) Accretionary dust mantles in CM chondrites:
837 Evidence for solar nebula processes. *Geochim. Cosmochim. Acta* **56**, 2873–2897.
- 838 Meyer H. J. (1984) The influence of impurities on the growth rate of calcite. *J. Cryst. Growth*
839 **66**, 639–646.
- 840 Morse J. W., Wang Q. and Tsio M. Y. (1997) Influences of temperature and Mg:Ca ratio on
841 CaCO_3 precipitates from seawater. *Geology* **25**, 85–87.
- 842 Organova N. I., Drits V. A. and Dmitrik A. L. (1972) Structural study of tochilinite. Part I.
843 The isometric variety. *Kristallografiya* **17**, 761–767.
- 844 Palme H., Lodders K. and Jones A. (2014) Solar System Abundances of the Elements A2 -
845 Holland, Heinrich D. In *Treatise on Geochemistry (Second Edition)* (ed. K. K.
846 Turekian). Elsevier, Oxford. pp. 15–36.
- 847 Petit M., McKeegan K., Gounelle M., Mostefaoui S., Marrocchi Y., Meibom A. and Leshin
848 L. A. (2009) Duration and sequence of carbonate crystallization on the Orgueil
849 protolith: ^{53}Mn – ^{53}Cr systematics of their evolution in O and C isotopic composition.
850 *Lunar Planet Sci* **40**, 1657.
- 851 Piani L., Robert F. and Remusat L. (2015) Micron-scale D/H heterogeneity in chondrite
852 matrices: A signature of the pristine solar system water? *Earth Planet. Sci. Lett.* **415**,
853 154–164.
- 854 Piani L., Yurimoto H. and Remusat L. (2017) A dual origin for water in the CM carbonaceous
855 chondrites. *Lunar Planet. Sci.* **48**. Lunar Planet. Inst., Houston. #1203 (abstr.).

- 856 Pignatelli I., Marrocchi Y., Vacher L. G., Delon R. and Gounelle M. (2016) Multiple
857 precursors of secondary mineralogical assemblages in CM chondrites. *Meteorit.*
858 *Planet. Sci.* **51**, 785–805.
- 859 Pignatelli I., Marrocchi Y., Mugnaioli E., Bourdelle F. and Gounelle M. (2017)
860 Mineralogical, crystallographic and redox features of the earliest stages of fluid
861 alteration in CM chondrites. *Geochim. Cosmochim. Acta* **209**, 106–122.
- 862 Remusat L., Robert F., Meibom A., Mostefaoui S., Delpoux O., Binet L., Gourier D. and
863 Derenne S. (2009) Protoplanetary disk chemistry recorded by D-rich organic radicals
864 in carbonaceous chondrites. *Astrophys. J.* **698**, 2087-2092.
- 865 Robinson D. N. (1975) Magnetite-serpentine-calcite dykes at Premier Mine and aspects of
866 their relationship to kimberlite and to carbonatite of alkalic carbonatite complexes.
867 *Phys. Chem. Earth* **9**, 61–70.
- 868 Rollion-Bard C., Mangin D. and Champenois M. (2007) Development and Application of
869 Oxygen and Carbon Isotopic Measurements of Biogenic Carbonates by Ion
870 Microprobe. *Geostand. Geoanalytical Res.* **31**, 39–50.
- 871 Rubin A. E. (2015) An American on Paris: Extent of aqueous alteration of a CM chondrite
872 and the petrography of its refractory and amoeboid olivine inclusions. *Meteorit.*
873 *Planet. Sci.* **50**, 1595–1612.
- 874 Rubin A. E., Trigo-Rodríguez J. M., Huber H. and Wasson J. T. (2007) Progressive aqueous
875 alteration of CM carbonaceous chondrites. *Geochim. Cosmochim. Acta* **71**, 2361–
876 2382.
- 877 Sephton, M. A. (2002) Organic Compounds in Carbonaceous Meteorites. *Natural Product*
878 *Rep.* **19**, 292–311.
- 879 Sofe M. (2013) The oldest carbonate minerals on Earth: Insights into the early history of the
880 Solar System. Ph. D. thesis, Univ. Glasgow.
- 881 Safronov V. S. (1969) Evolution of the Protoplanetary Cloud and Formation of the Earth and
882 Planets. Nauka (Transl. Israel Program for Scientific Translations. NASA 'ITF-677,
883 1972).
- 884 Steer E. D. and Treiman H. (2014) Alteration of sulphides in the Rumuruti chondrite LAP
885 031275. In *77th Annual Meeting of the Meteoritical Society*. #5333 (abstr.).
- 886 Tomeoka K. and Buseck P. R. (1985) Indicators of aqueous alteration in CM carbonaceous
887 chondrites: Microtextures of a layered mineral containing Fe, S, O and Ni. *Geochim.*
888 *Cosmochim. Acta* **49**, 2149–2163.
- 889 Travis B. J. and Schubert G. (2005) Hydrothermal convection in carbonaceous chondrite
890 parent bodies. *Earth Planet. Sci. Lett.* **240**, 234–250.
- 891 Tsutsui S. and Naraoka H. (2008) Isotope Variation at Nanomolar Carbonate in the
892 Murchison Meteorite. *Meteorit. Planet. Sci. Suppl.* **43**, A5172.
- 893 Tsutsui S. and Naraoka H. (2009) Oxygen isotope variation at nanomolar carbonate in the

- 894 CM2 carbonaceous chondrites. *Meteorit. Planet. Sci. Suppl.* **44**, A5266.
- 895 Tyra M. A., Farquhar J., Guan Y. and Leshin L. A. (2012) An oxygen isotope dichotomy in
896 CM2 chondritic carbonates—A SIMS approach. *Geochim. Cosmochim. Acta* **77**, 383–
897 395.
- 898 Tyra M., Brearley A. and Guan Y. (2016) Episodic carbonate precipitation in the CM
899 chondrite ALH 84049: An ion microprobe analysis of O and C isotopes. *Geochim.*
900 *Cosmochim. Acta* **175**, 195–207.
- 901 Vacher L. G., Marrocchi Y., Verdier-Paoletti M. J., Villeneuve J. and Gounelle M. (2016)
902 Inward radial mixing of interstellar water ices in the solar protoplanetary disk.
903 *Astrophys. J.* **827**, L1.
- 904 Van Santen R. A. (1984) The Ostwald step rule. *J. Phys. Chem.* **88**, 5768–5769.
- 905 Verdier-Paoletti M.J., Marrocchi Y., Avice G, Roskosz M., Gurenko A. and Gounelle C.
906 (2017) Oxygen isotope constraints on the alteration temperatures of CM chondrites.
907 *Earth Planet. Sci. Lett.* **458**, 273-281.
- 908 Vinogradoff V., Remusat L., Bernard S. and Le Guillou C. (2015) The Insoluble Organic
909 Matter of the Paris CM Chondrite. In *78th Annual Meeting of the Meteoritical Society*
910 LPI Contributions. #5032 (abstr.).
- 911 Walter L. M. (1986) Relative efficiency of carbonate dissolution and precipitation during
912 diagenesis: a progress report on the role of solution chemistry. In Gautier, Donald L.,
913 ed. *Roles of Organic Matter in Sediment Diagenesis*. SEPM Special Publication, Vol.
914 38, 1986.
- 915 Wenner D. B. and Taylor H. P. (1971) Temperatures of serpentinization of ultramafic rocks
916 based on O^{18}/O^{16} fractionation between coexisting serpentine and magnetite. In
917 *Contributions to Mineralogy and Petrology* **32**, 165-187.
- 918 Wilson, L., K. Keil, L. B. Browning, A. N. Krot, and W. Bourcier. (1999) Early Aqueous
919 Alteration, Explosive Disruption, and Reprocessing of Asteroids. *Meteorit. Planet.*
920 *Sci.* **34**, 541–557.
- 921 Young E. D. (2001a) The hydrology of carbonaceous chondrite parent bodies and the
922 evolution of planet precursors. In Eleventh Annual VM Goldschmidt Conference. p.
923 3589.
- 924 Young E. D. (2001b) The hydrology of carbonaceous chondrite parent bodies and the
925 evolution of planet progenitors. *Philos. Trans. R. Soc. Lond. Math. Phys. Eng. Sci.*
926 **359**, 2095–2110.
- 927 Young E. D. (2004) The role of water in determining the oxygen isotopic composition of
928 planets. In Workshop on Oxygen in the Terrestrial Planets. p. 3051.
- 929 Young E. D., Ash R. D., England P. and Rumble D. (1999) Fluid Flow in Chondritic Parent
930 Bodies: Deciphering the Compositions of Planetesimals. *Science* **286**, 1331–1335.
- 931 Young E. D., Zhang K. K. and Schubert G. (2003) Conditions for pore water convection

932 within carbonaceous chondrite parent bodies – implications for planetesimal size and
933 heat production. *Earth Planet. Sci. Lett.* **213**, 249–259.

934 Yuen G., Blair N., Des Marais D. J. and Chang S. (1984) Carbon isotope composition of low
935 molecular weight hydrocarbons and monocarboxylic acids from Murchison meteorite.
936 *Nature* **307**, 252–254.

937 Zolensky M. E., Barrett R. and Browning L. (1993) Mineralogy and composition of matrix
938 and chondrule rims in carbonaceous chondrites. *Geochim. Cosmochim. Acta* **57**, 3123–
939 3148.

940 Zolensky M. E., Mittlefehldt D. W., Lipschutz M. E., Wang M.-S., Clayton R. N., Mayeda T.
941 K., Grady M. M., Pillinger C. and B. D. (1997) CM chondrites exhibit the complete
942 petrologic range from type 2 to 1. *Geochim. Cosmochim. Acta* **61**, 5099–5115.

943

944 **Figure captions**

945

946 **Figure 1:** a) Raman spectra in the 100-1500 cm⁻¹ region of a typical calcite in Paris. b) Raman
947 spectra in the 100-1500 cm⁻¹ region of a typical aragonite in Paris. c) Raman spectra in the
948 200-1000 cm⁻¹ region of tochilinite rims around Ca-carbonates (purple line) and reference
949 Raman spectra of an unoriented crystal of tochilinite (785nm) from the RUFF database
950 (RUFF ID 060887, black line).

951

952 **Figure 2:** New petrographic types classification of Ca-carbonates for CM chondrites with
953 petrologic subtypes between 2.7 and 2.3 (modified after Lee et al., (2014)). Type 0 was added
954 from the previous classification and refers to Ca-carbonate without tochilinite/cronstedtite rim
955 where all the edges of the crystal or the grain are in direct contact with the matrix. Aragonite
956 classification was divided into two subtypes, Type 1a that occur for instance only in Paris and
957 Type 0 that corresponds to the previous description of aragonite report by Lee et al., (2014).

958

959 **Figure 3:** Back-scattered electron image (BSE) of Type 1a subhedral aragonite grain (A)
960 surrounded by tochilinite-cronstedtite associations (TCI). The dash ellipse denotes the area of

961 the $\delta^{13}\text{C}$ ion probe spot. b) BSE image of polycrystalline Type 1a calcite grains (C) with
962 euhedral, subhedral and anhedral shapes surrounded by TCI rim. c) BSE image of an anhedral
963 Type 1a calcite grain (C) partially enclosed by a TCI rim. d) BSE image of a polycrystalline
964 Type 1a calcite (C) equant grain surrounding by a TCI rim.

965

966 **Figure 4:** a) to d) Back-scattered electron images of Type 1a calcite (C) and Ca-carbonate
967 (Cc) grains surrounded by TCI rims or magnetite (Mt) with euhedral shapes and crystal faces
968 parallel or subparallel to the central Ca-carbonate. e) Back-scattered electron images of a
969 Type 1a Ca-carbonate (Cc) grain fractured into three parts, each of which shows a different
970 stages of replacement: (1) beginning of replacement of the Ca-carbonate (Cc), (2) almost
971 complete dissolution and replacement of the Ca-carbonate by TCI, and (3) complete
972 replacement of the Ca-carbonate by TCI. f) EDX elemental map showing the distribution of
973 Ca (in yellow), revealing the Ca-rich nature of the TCI precursor.

974

975 **Figure 5:** a) BSE image of a Type 0 euhedral aragonite grain (A). b) BSE image of
976 polycrystalline Type 0 aragonite (A) equant grain. c) BSE image of subhedral and anhedral
977 fractured Type 0 calcite grains (C). d) BSE image of a group of Type 0 calcite (C) grains that
978 are several hundred of microns in size.

979

980 **Figure 6:** $\delta^{13}\text{C}$ values of Type 1a calcite (blue circles), Type 1a aragonite (blue diamonds),
981 Type 0 calcite (green circles) and Type 0 aragonite (green diamonds) from this study (errors =
982 2σ).

983

984 **Figure 7:** Oxygen three-isotope plot for Type 1a calcite (blue circles), Type 1a aragonite
985 (blue diamonds), Type 0 calcite (green circles) and Type 0 aragonite (green diamonds) from

986 this study and from Vacher et al., 2016 (errors = 2σ). The data from the literature (grey
987 circles) are also shown with 2σ typical errors (Benedix et al., 2003; Tyra et al., 2012, 2016;
988 Lee et al., 2013; Horstmann et al., 2014; Fujiya et al., 2015; Vacher et al., 2016; Lindgren et
989 al., 2017). TFL: Terrestrial Fractionation Line, $\delta^{17}\text{O} = 0.52 \times \delta^{18}\text{O}$. CMW: CM Water line,
990 $\delta^{17}\text{O} = 0.69 \times \delta^{18}\text{O} - 2.12$ (Verdier-Paoletti et al., 2017). CCAM: Carbonaceous Chondrite
991 Anhydrous Mineral line, $\delta^{17}\text{O} = 0.941 \times \delta^{18}\text{O} - 4$. YR: Young and Russell line, $\delta^{17}\text{O} = \delta^{18}\text{O}$.

992

993 **Figure 8:** $\delta^{13}\text{C}$ values of Ca-carbonates from this study and from the literature (light green)
994 (Grady et al., 1988; Guo and Eiler, 2007; Alexander et al., 2015; Fujiya et al., 2015; Tyra et
995 al., 2016). The $\delta^{13}\text{C}$ values of the potential C sources at the origin of the ^{13}C enrichment in
996 CM carbonates are also plotted. The blue data-point corresponds to the average $\delta^{13}\text{C}$ value of
997 inorganic carbonaceous ices from Manfroid et al. (2009). The $\delta^{13}\text{C}$ values of presolar grains
998 are represented in purple (Amari et al., 2014; Davidson et al., 2014), the $\delta^{13}\text{C}$ values of
999 soluble organic matter are in red (Sephton, 2002 and *references therein; Aponte et al., 2016),
1000 the $\delta^{13}\text{C}$ values of insoluble organic matter are in yellow (Sephton, 2002 and *references
1001 therein; Alexander et al., 2007, 2010; Hashizume et al., 2011; Vinogradoff et al., 2015), and
1002 the predicted $\delta^{13}\text{C}$ values of CM carbonates that precipitated from a single fluid in
1003 equilibrium with water and C-bearing gases are in brown (Alexander et al., 2015).

1004

1005 **Figure 9:** $\delta^{13}\text{C}$ vs $\delta^{18}\text{O}$ values of Ca-carbonates measured in this study. Although a positive
1006 trend can be observed, the high MSWD (115) suggest that it rather correspond to two
1007 different clusters characterized by ^{13}C - $^{17,18}\text{O}$ -rich and ^{12}C - ^{16}O -rich Ca-carbonates,
1008 respectively.

1009

1010 **Figure 10:** (a) $\delta^{13}\text{C}$ vs $\delta^{18}\text{O}$ values for Type 1a calcite (blue circles), Type 1a aragonite (blue
1011 diamonds), Type 0 calcite (green circles) and Type 0 aragonite (green diamonds) from this
1012 study. The solid black line represents the linear regression ($R^2 = 0.71$, $n = 14$) in our dataset:
1013 $\delta^{13}\text{C} = (5.0 \pm 1.8) \times \delta^{18}\text{O} - (128 \pm 65)$. The dash lines represent the confidence level of the
1014 linear regression (1σ). The white circle line is the predicted isotopic compositions of CM
1015 carbonates as a function of temperature (between 0°C and 130°C) in a $\text{CO-H}_2\text{O}$ system
1016 ($\delta^{13}\text{C}_{\text{CO}} = -33 \text{‰}$ and $\delta^{18}\text{O}_{\text{H}_2\text{O}} = 5 \text{‰}$) (Alexander et al., 2015). The white circles on the model
1017 mark 10°C intervals. (b) $\delta^{13}\text{C}$ vs $\delta^{18}\text{O}$ values of Ca-carbonates in this study. The white circle
1018 lines are the predicted isotopic compositions of CM carbonates as a function of temperature
1019 (between 0°C and 130°C) and the mole fraction of CO_2 in a $\text{CO-CO}_2\text{-H}_2\text{O}$ system ($\delta^{13}\text{C}_{\text{CO}} = -$
1020 5‰ and $\delta^{18}\text{O}_{\text{H}_2\text{O}} = 5 \text{‰}$) (Alexander et al., 2015). The white circles on the model mark 10°C
1021 intervals.

1022
1023 **Figure 11:** (a) Possible $\delta^{13}\text{C}$ - $\delta^{18}\text{O}$ values of alteration fluids estimated by (i) considering O-
1024 isotopic equilibrium between $^{17,18}\text{O}$ -rich fluid (red star; PW = Primordial Water) and ^{16}O -rich
1025 anhydrous silicates (red hexagon) and (ii) assuming two ^{12}C - and ^{13}C -rich end-members of
1026 soluble organic matter as plausible sources of carbon for carbonate precipitation. The blue
1027 lines correspond to the CM water line (CMW) that results from the equilibration between
1028 primordial water and anhydrous silicates (Clayton and Mayeda, 1984; Clayton and Mayeda,
1029 1999; Verdier-Paoletti et al., 2017). The fractionation factor α for O-isotopes between fluids
1030 and precipitated carbonates is also represented for different temperatures (Kim and O'Neil,
1031 1997). It should be noted that fractionation factor between Ca-carbonate and carbonate ion in
1032 the fluids is negligible over a large temperature range (Deines et al., 1974; Luo and Wang,
1033 2009). (b) $\delta^{13}\text{C}$ vs $\delta^{18}\text{O}$ values for Type 1a calcite (blue circles), Type 1a aragonite (blue
1034 diamonds), Type 0 calcite (green circles) and Type 0 aragonite (green diamonds) from this

1035 study. We also represented the *in situ* $\delta^{13}\text{C}$ - $\delta^{18}\text{O}$ reported in previous studies (Fujiya et al.,
1036 2015; Tyra et al., 2016). Assuming an average temperature precipitation of Ca-Carbonates of
1037 110°C (Fujiya et al., 2015; Tyra et al., 2016), our model reproduces the range of $\delta^{13}\text{C}$ - $\delta^{18}\text{O}$
1038 observed in Paris and reported in other CM chondrites (Fujiya et al., 2015; Tyra et al., 2016).

1039

1040

1041

1042

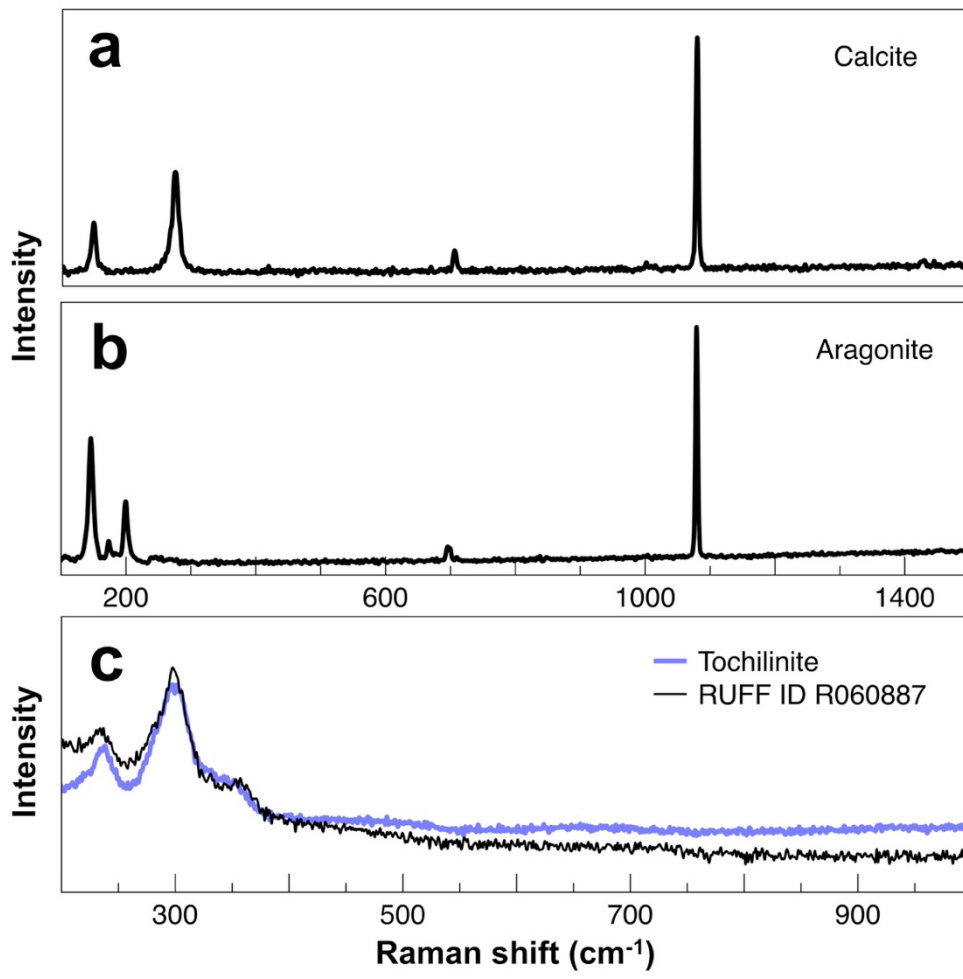


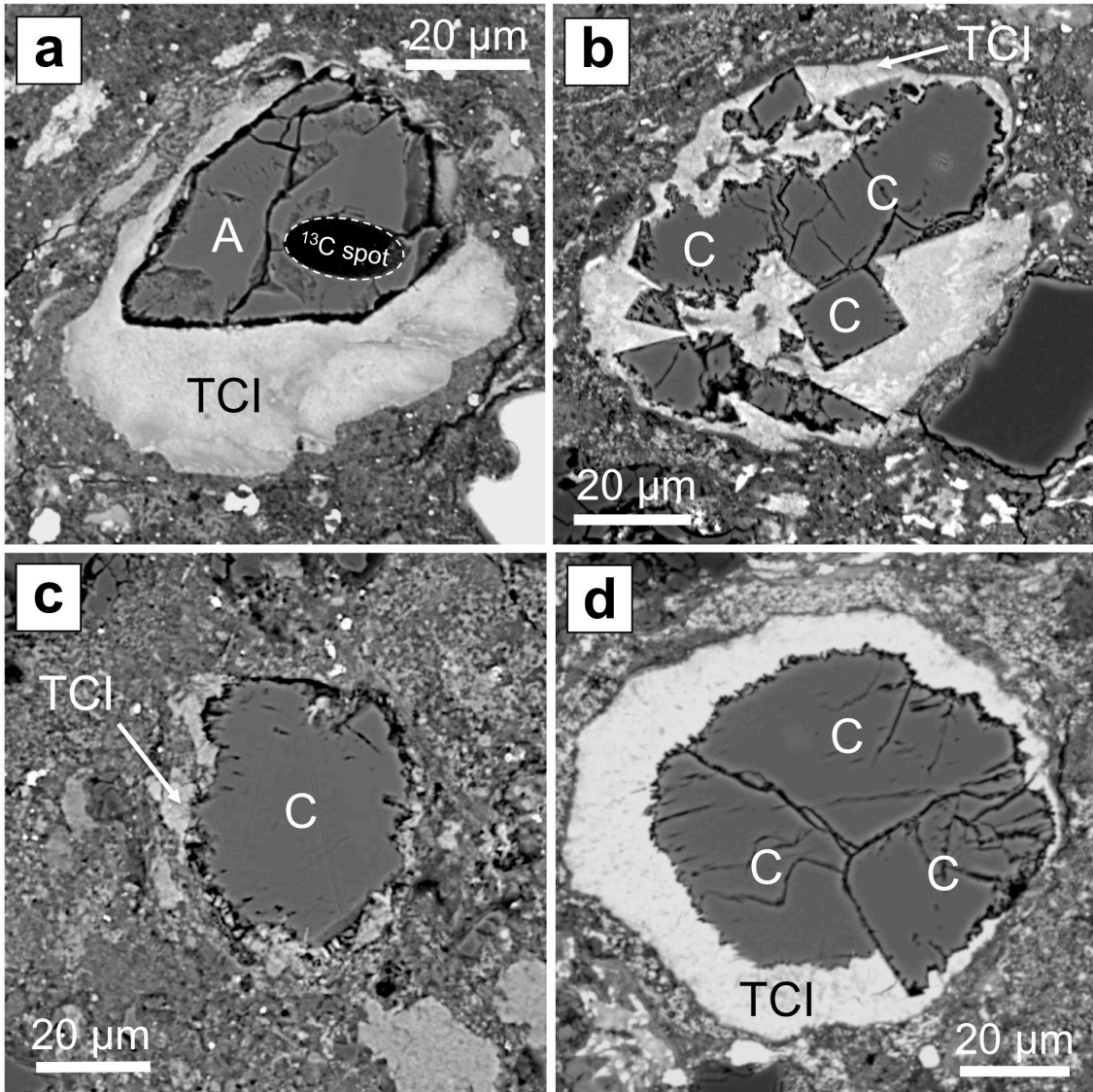
Fig. 1

| | Aragonite | | ← Calcite → | | | | | | |
|--------|------------------|-----------|--------------------|-----------|-----------|-----------|-----------|--|--------------------------------------|
| | <i>0</i> | <i>1a</i> | <i>0</i> | <i>1a</i> | <i>1b</i> | <i>2a</i> | <i>2b</i> | | <i>Vein</i> |
| CM 2.7 | | | | | | | | | Paris |
| CM 2.5 | | | | | | | | | EET 96029 Murchison |
| CM 2.4 | | | | | | | | | Murray Pollen |
| CM 2.3 | | | | | | | | | Mighei LON 94101 |

1046

1047

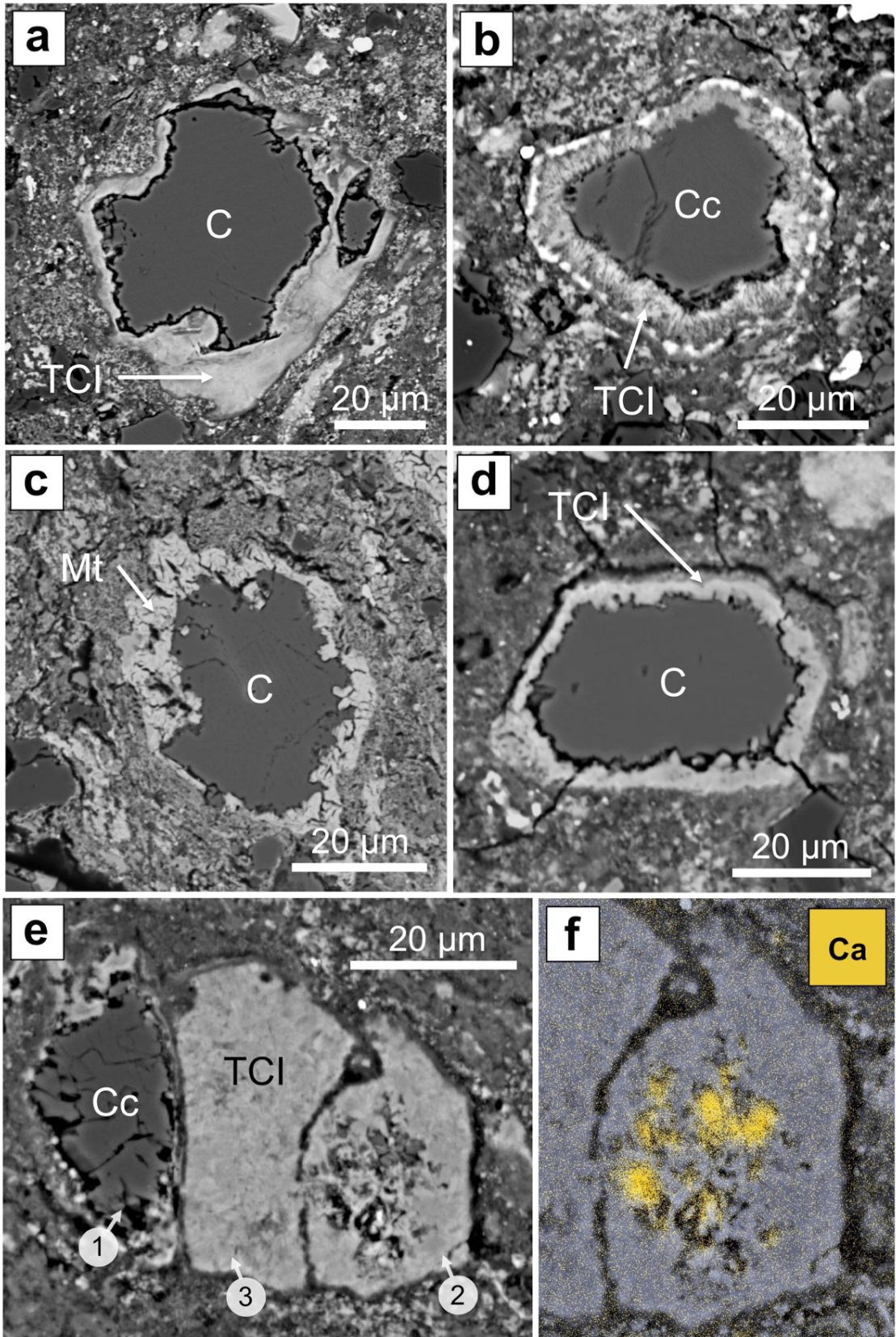
Fig. 2



1048

1049

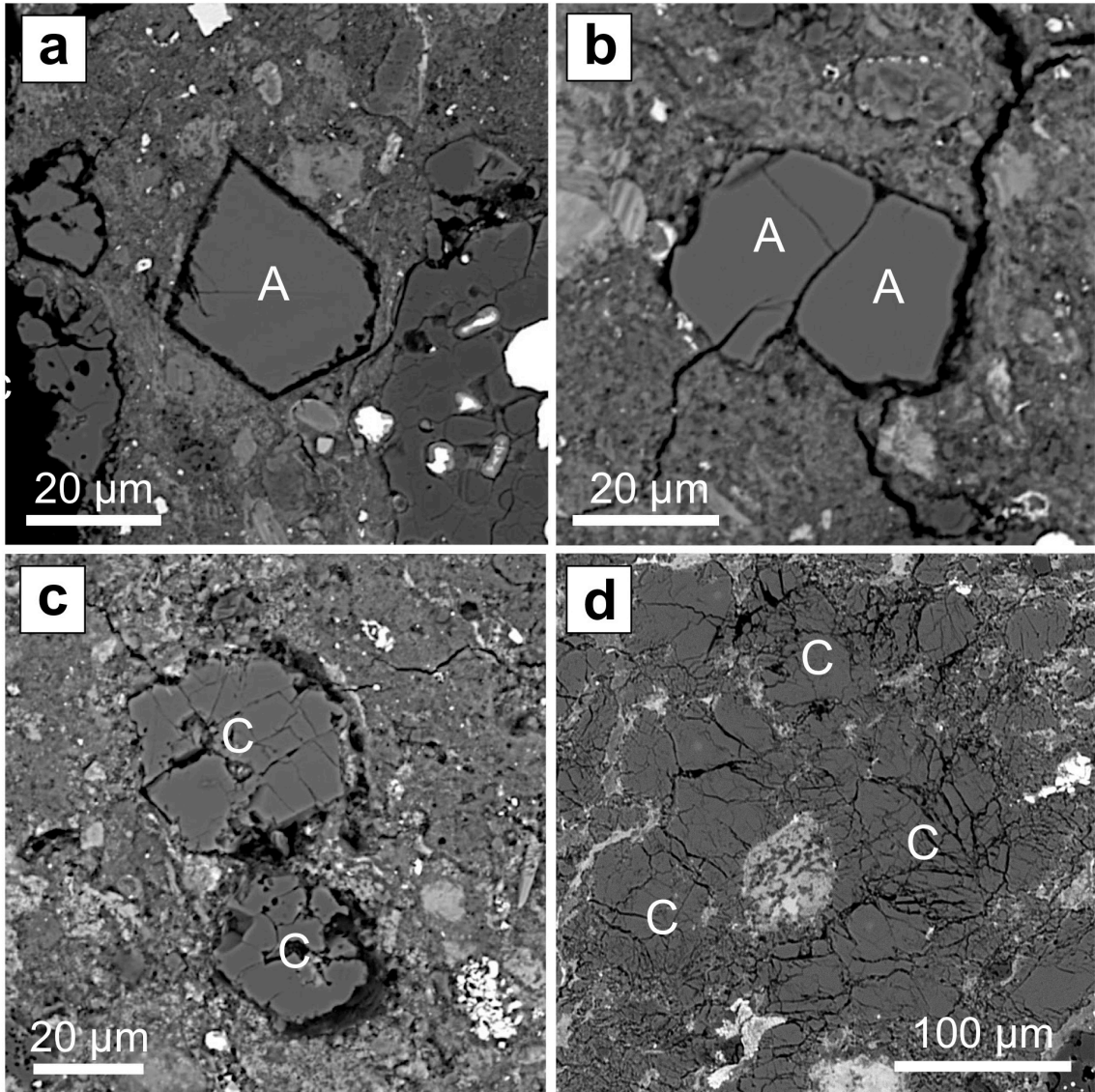
Fig. 3



1050

1051

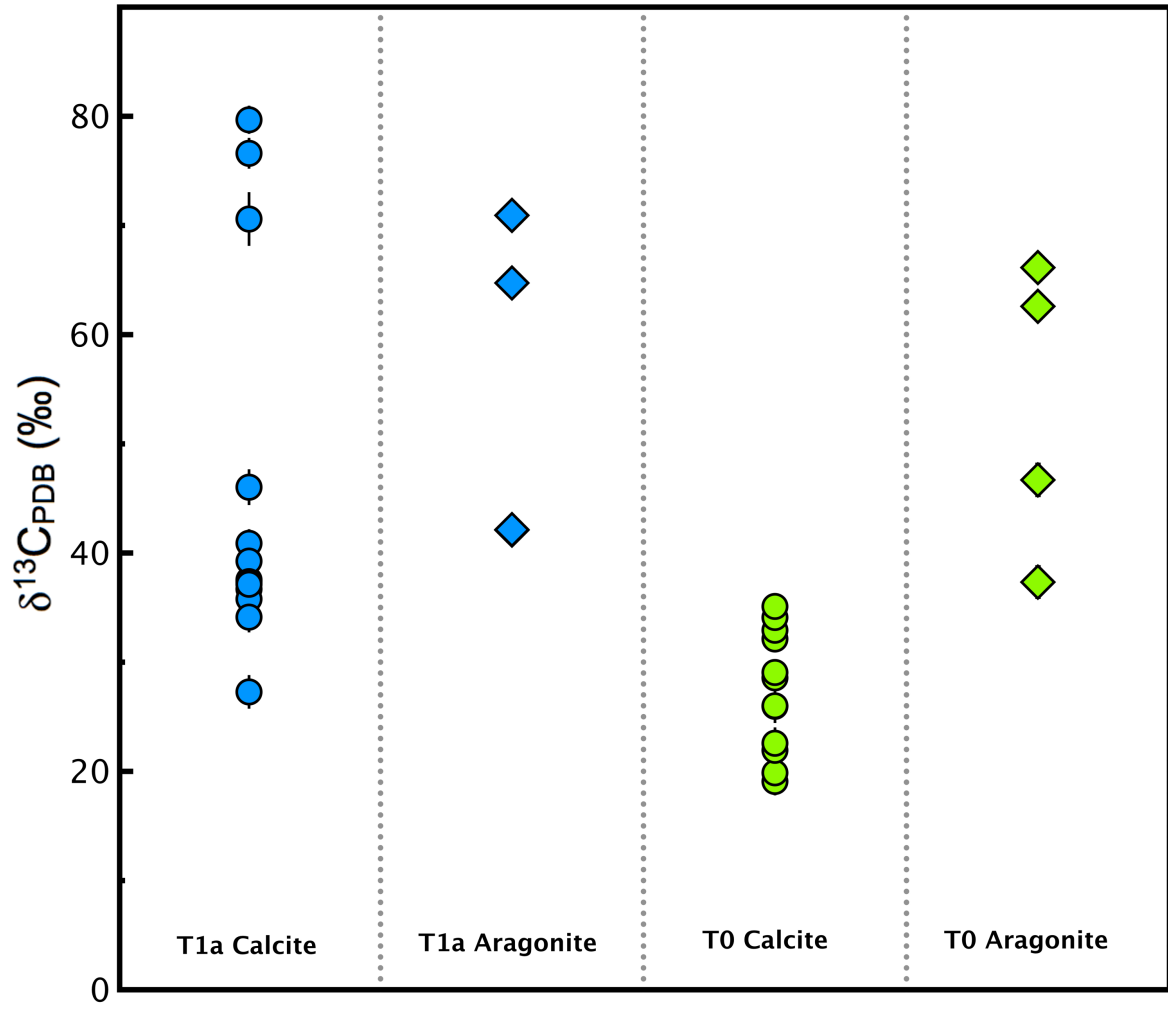
Fig. 4



1052

1053

Fig. 5



1054

1055

Fig. 6

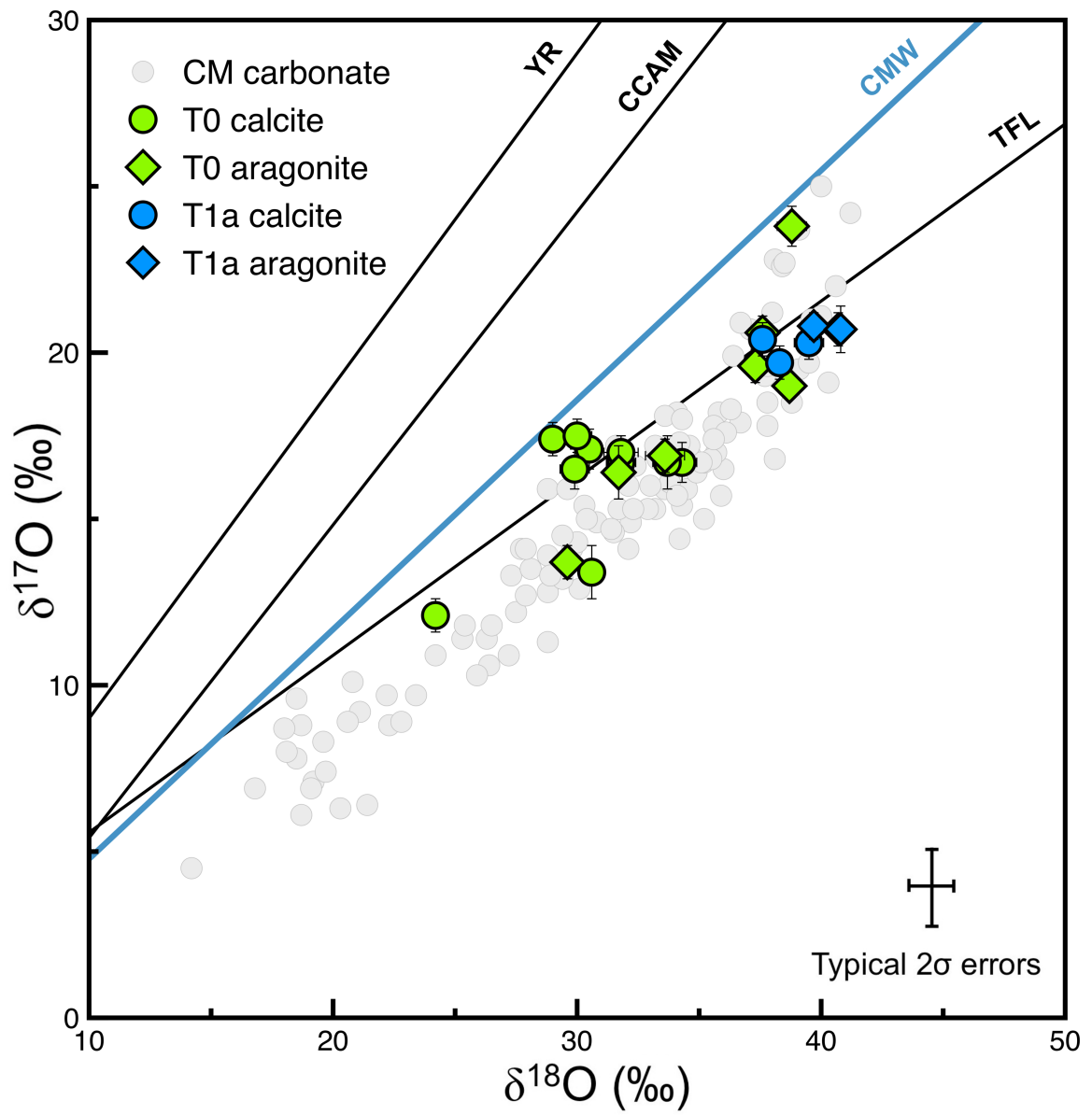
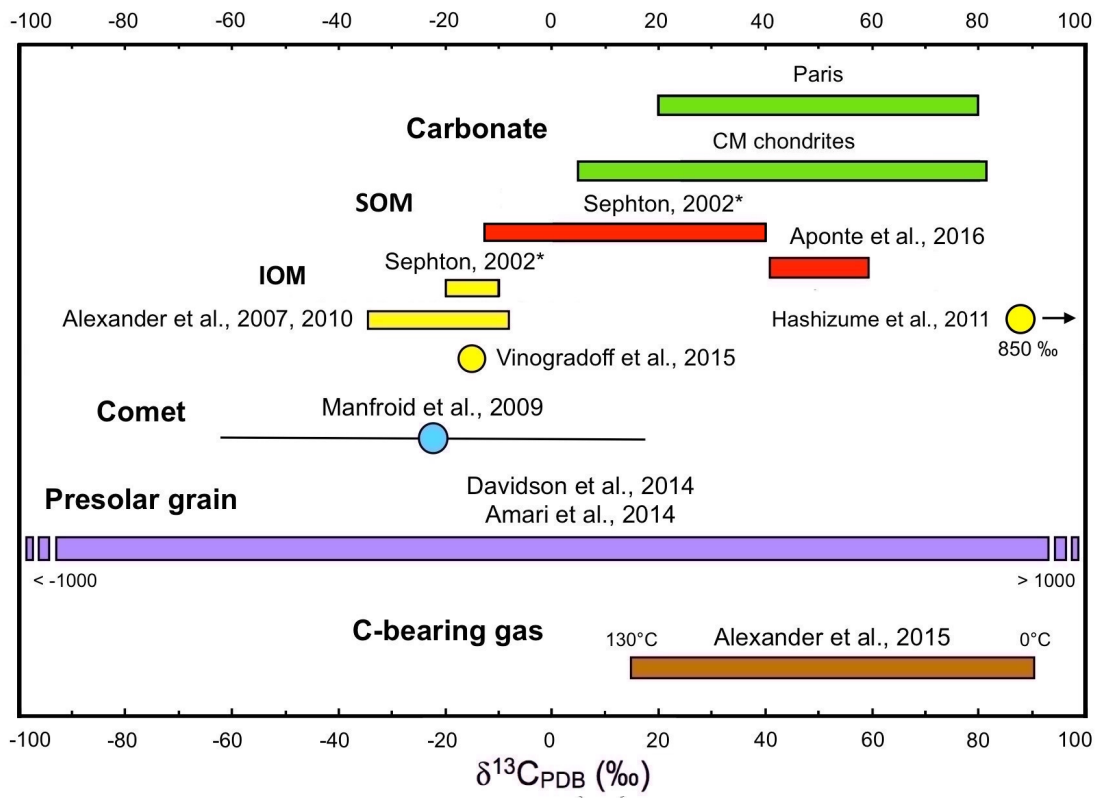


Fig. 7

1056
1057

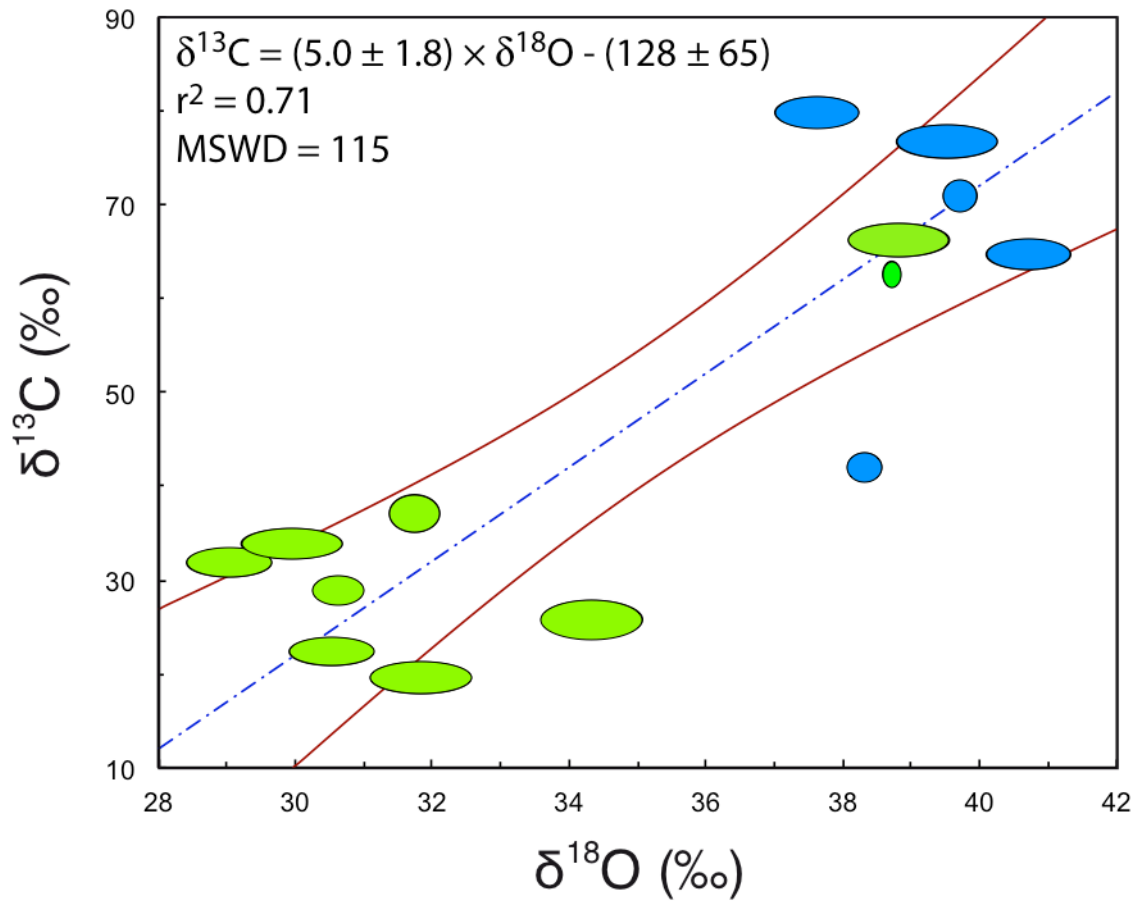


1058

1059

1060

Fig. 8

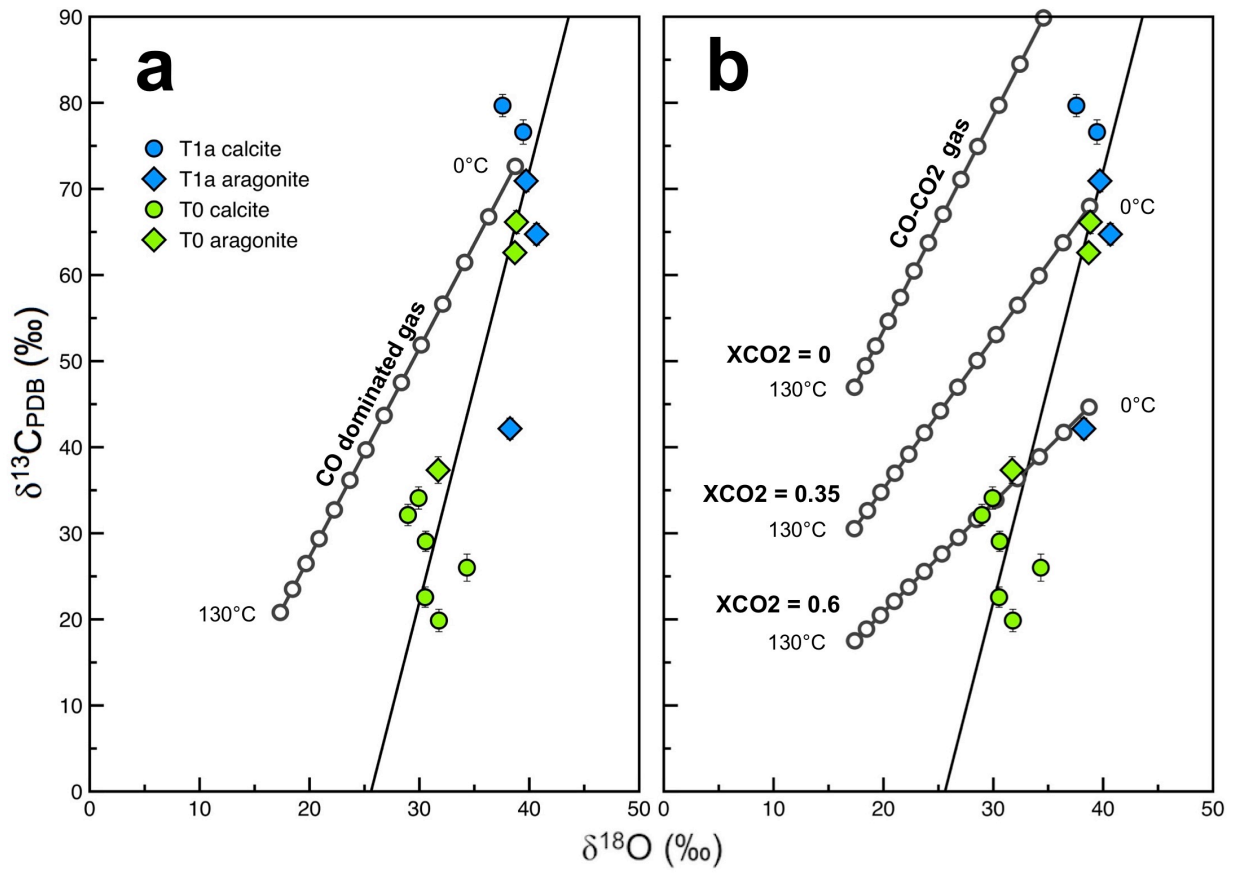


1061

1062

1063

Fig. 9

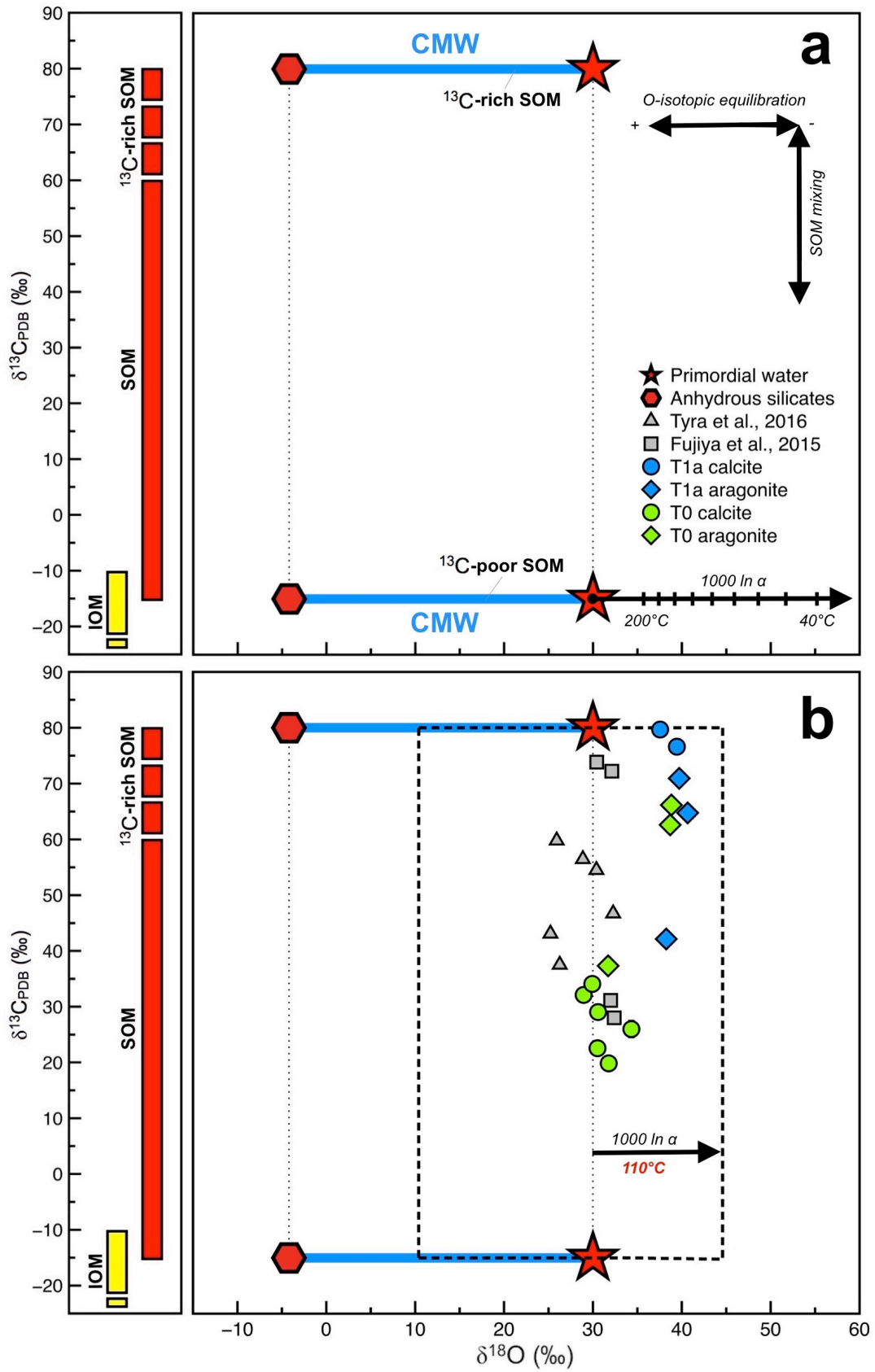


1064

1065

1066

Fig. 10



1067

1068

1069

Fig. 11

| # | Type | Polymorph | Area | $\delta^{13}\text{C}$ (‰) | 2 σ | $\delta^{18}\text{O}$ (‰) | 2 σ | $\delta^{17}\text{O}$ (‰) | 2 σ | $\Delta^{17}\text{O}$ | 2 σ |
|--------------|------|-----------|---------|---------------------------|------------|---------------------------|------------|---------------------------|------------|-----------------------|------------|
| C1 | 1a | Calcite | Altered | 27.3 | 1.5 | | | | | | |
| C2 | 1a | Calcite | Altered | 34.1 | 1.4 | | | | | | |
| C3 | 1a | Calcite | Altered | 35.8 | 1.4 | | | | | | |
| C4 | 1a | Calcite | Altered | 36.7 | 1.3 | | | | | | |
| C5 | 1a | Calcite | Altered | 37.1 | 1.4 | | | | | | |
| C6 | 1a | Calcite | Altered | 37.4 | 1.4 | | | | | | |
| C7 | 1a | Calcite | Altered | 37.6 | 1.4 | | | | | | |
| C8 | 1a | Calcite | Altered | 39.3 | 1.2 | | | | | | |
| C9 | 1a | Calcite | Altered | 40.9 | 1.3 | | | | | | |
| A10 | 1a | Aragonite | Altered | 42.1 | 1.3 | | | | | | |
| #27* | 1a | Aragonite | Fresh | 42.2 | 1.2 | 38.3 | 0.2 | 19.7 | 0.5 | -0.2 | 0.4 |
| C11 | 1a | Calcite | Altered | 46 | 1.6 | | | | | | |
| #34* | 1a | Aragonite | Fresh | 64.7 | 1.3 | 40.7 | 0.5 | 20.7 | 0.5 | -0.5 | 0.4 |
| C12 | 1a | Calcite | Fresh | 70.6 | 2.5 | | | | | | |
| #33* | 1a | Aragonite | Fresh | 70.9 | 1.3 | 39.7 | 0.2 | 20.8 | 0.4 | 0.1 | 0.4 |
| #31* | 1a | Calcite | Fresh | 76.6 | 1.4 | 39.5 | 0.6 | 20.3 | 0.5 | -0.2 | 0.4 |
| #24* | 1a | Calcite | Fresh | 79.7 | 1.3 | 37.6 | 0.5 | 20.4 | 0.5 | 0.9 | 0.4 |
| #35* | 1a | Aragonite | Altered | | | 40.8 | 0.1 | 20.7 | 0.7 | -0.5 | 0.6 |
| Mean | | | | 48.2 | | 39.4 | | 20.4 | | -0.1 | |
| <i>StDev</i> | | | | <i>16.9</i> | | <i>1.3</i> | | <i>0.4</i> | | <i>0.5</i> | |
| C13 | 0 | Calcite | Altered | 19.1 | 1.3 | | | | | | |
| #12* | 0 | Calcite | Altered | 19.9 | 1.3 | 31.8 | 0.6 | 16.7 | 0.6 | 0.2 | 0.5 |
| C14 | 0 | Calcite | Altered | 21.9 | 2.1 | | | | | | |
| C15 | 0 | Calcite | Altered | 22.6 | 1.2 | 30.5 | 0.5 | 17.1 | 0.6 | 1.2 | 0.4 |
| C16 | 0 | Calcite | Altered | 26 | 1.4 | | | | | | |
| #20* | 0 | Calcite | Altered | 26 | 1.6 | 34.3 | 0.6 | 16.7 | 0.6 | -1.2 | 0.4 |
| C17 | 0 | Calcite | Altered | 28.6 | 1.3 | | | | | | |
| C18 | 0 | Calcite | Altered | 29.1 | 1.2 | 30.6 | 0.3 | 13.4 | 0.8 | -2.5 | 0.7 |
| C19 | 0 | Calcite | Altered | 32.1 | 1.2 | 29 | 0.5 | 17.4 | 0.5 | 2.3 | 0.4 |
| C20 | 0 | Calcite | Altered | 32.9 | 1.4 | | | | | | |
| C21 | 0 | Calcite | Altered | 34.1 | 1.3 | 29.9 | 0.6 | 16.5 | 0.6 | 1 | 0.4 |
| C22 | 0 | Calcite | Altered | 35.1 | 1.2 | | | | | | |
| #11* | 0 | Aragonite | Fresh | 37.3 | 1.6 | 31.7 | 0.3 | 16.4 | 0.8 | 0 | 0.3 |
| A23 | 0 | Aragonite | Fresh | 46.7 | 1.6 | | | | | | |
| #28* | 0 | Aragonite | Fresh | 62.6 | 1.1 | 38.7 | 0.1 | 19 | 0.4 | -1.1 | 0.3 |
| #29* | 0 | Aragonite | Fresh | 66.2 | 1.4 | 38.8 | 0.6 | 23.8 | 0.6 | 3.6 | 0.5 |
| #1* | 0 | Calcite | Fresh | | | 24.2 | 0.2 | 12.1 | 0.5 | -0.5 | 0.4 |
| #7* | 0 | Aragonite | Fresh | | | 29.6 | 0.2 | 13.7 | 0.5 | -1.7 | 0.4 |
| #13* | 0 | Calcite | Altered | | | 31.8 | 0.7 | 17.0 | 0.5 | 0.5 | 0.4 |
| #18* | 0 | Aragonite | Fresh | | | 33.6 | 0.8 | 16.9 | 0.5 | -0.6 | 0.4 |
| #19* | 0 | Calcite | Altered | | | 33.7 | 0.6 | 16.7 | 0.8 | -0.8 | 0.6 |
| #23* | 0 | Aragonite | Altered | | | 37.3 | 0.1 | 19.6 | 0.5 | 0.2 | 0.4 |
| #25* | 0 | Aragonite | Fresh | | | 37.6 | 0.2 | 20.6 | 0.5 | 1.0 | 0.7 |
| C24 | 0 | Calcite | Altered | | | 30.0 | 0.6 | 17.5 | 0.5 | 1.9 | 0.4 |
| Mean | | | | 33.8 | | 32.5 | | 17.1 | | 0.2 | |
| <i>StDev</i> | | | | <i>13.9</i> | | <i>3.9</i> | | <i>2.7</i> | | <i>1.5</i> | |

1070

1071 **Table 1.** Carbon and oxygen isotopic compositions of Paris Ca-carbonates. $\Delta^{17}\text{O}$ errors were
1072 calculated using the errors in the $^{17}\text{O}/^{18}\text{O}$ ratio. *Same grain as the study of Vacher et al.,
1073 (2016).

1074

1075